J. Fluid Mech. (1994), *vol.* 279, *pp.* 239–278

Density fluctuation correlations in free turbulent binary mixing

By P. CHASSAING[1], G. HARRAN[2] AND L. JOLY[3]

[1]Institut National Polytechnique, ENSEEIHT, 2 rue Camichel, 31000 Toulouse, France.

[2]Institut de Mécanique des Fluides, avenue du Professeur C. Soula, 31400 Toulouse, France.

[3]ENSICA, 49 avenue L. Blum 31056 Toulouse, France.

(Received 21 July 1993 and in revised form 19 May 1994)

This paper is devoted to the analysis of the turbulent mass flux and, more generally, of the density fluctuation correlation (d.f.c.) effects in variable-density fluid motion. The situation is restricted to the free turbulent binary mixing of an inhomogeneous round jet discharging into a quiescent atmosphere. Based on conventional (Reynolds) averaging, a ternary regrouping of the correlations occurring in the statistical averaging of the open equations is first introduced. Then an exact algebraic relationship between the d.f.c. terms and the second-order moments is demonstrated. Some consequences of this result on the global behaviour of variable-density jets are analytically discussed. The effects of the d.f.c. terms are shown to give a qualitative explanation of the influence of the ratio of the densities of the inlet jet and ambient fluid on the centerline decay rates of mean velocity and mass fraction, the entrainment rate and the restructuring of the jet. Finally, the sensitivity of second-order modelling to the d.f.c. terms is illustrated and it is suggested that such terms should be considered as independent variables in the closing procedure.

1. Introduction

When averaging the constant-density Navier–Stokes equations, the nonlinearity of the advection term introduces the well-known Reynolds stresses or double velocity fluctuation correlations. With the same type of approach, new additional correlations appear in the variable-density turbulent flow case compared to the constant-density one. These terms are basically density fluctuation correlation (d.f.c.) terms, which occur from the additional nonlinearities associated with the density variation. There are still a lot of questions about these terms concerning (i) the statistical averaging of the open set of equations, (ii) the modelling procedure and (iii) the experimental evidence.

As far as statistical averaging is concerned, at least four types of method have been proposed for studying variable-density turbulent flows. The first is the mass-weighted or Favre's averaging (1958, 1965*a*, *b*, 1971, 1975, 1992) which leads to an open system of equations formally similar to the constant-density case. The second is the mixed-weighted averaging introduced by Bauer, Zumwalt & Fila (1968) and developed by Ha Minh, Launder & Mac Innes (1981). The third is nothing more than conventional averaging, without or with approximations to the density fluctuation, as suggested for instance by Shih, Lumley & Janicka (1987) for the mass mixing, and by Rey & Rosant (1990) and Rey (1991) for thermal mixing. The last one was originally

proposed by Chassaing (1985) and can be viewed as an interlocking method based on centred fluctuations, according to Reynolds' averaging, but using some type of mass-weighted second-order moments, in analogy with Favre's averaging.

Turning now to the modelling procedure, and according to the formal incompressible analogy when using Favre's decomposition, the variable-density closure schemes are often developed as an extrapolation of those for the constant-density case. This was done by Vandromme & Ha Minh (1987) and Vandromme (1991) for instance, and, as reviewed by Cousteix & Aupoix (1989), by most authors. However, as recalled by Chen, Gouldin & Lumley (1987), it is not clear to what extent model assumptions which are justified for the incompressible case can be adopted for closure of density-weighted moments for variable-density flows. In fact, as shown by Shih *et al.*(1987), conventional models can be used to predict the mean properties of a variable-density turbulent mixing layer in fair agreement with the experimental data.

Concerning the experimental evidence, direct measurements of d.f.c. terms are rather scarce. Most of the available data concern simple turbulent shear flows, such as boundary layers and jets. They suggest that the $\overline{\rho' u'}$ correlation between the density fluctuation and the streamwise velocity fluctuation is generally low compared to the product of the mean values. Here an overbar denotes a classical statistical average of Reynolds' fluctuations. In a helium–air jet, Zhu, So & Otügen (1989) found that the maximum of the absolute centreline value of $\overline{\rho' u'}/\bar{\rho}\bar{U}$ was about 0.3×10^{-2}. This result was confirmed later by So *et al.*(1990). Similarly, the measurements of Larue & Libby (1977, 1980) in the turbulent boundary layer with slot injection of helium, give a maximum value of $\overline{\rho' u'}/\bar{\rho}\bar{U} \approx 1.4 \times 10^{-2}$. Concerning the $\overline{\rho' u'}$ and $\overline{\rho' v'}$ variations with respect to the mean density gradients, the study of Driscoll, Schefer & Dibble (1982) should be mentioned. From direct measurements of these quantities in a turbulent non-premixed flame, these authors drew the conclusion that a first gradient diffusion submodel for the closure of these correlations was inconsistant with the axial data. Concerning the mass fraction/density correlation, an interesting result emerges from the recent investigation of Sautet (1992). For pure H_2–air jet mixing, the density–concentration fluctuation $\overline{\rho' \gamma'}$ is negative. The absolute value along the axis is as much as 40% of $(\bar{\rho}\bar{C})_{\mathcal{L}}$ at the downstream location $x/D_0 = 18$. On the other hand, when the density ratio is greater than unity, as for the pure CO_2–air jet mixing, this correlation is found to be positive.

Thus, at the present time, there is no definitive experimental evidence to support or contradict the idea that quantities like $\bar{\rho}\bar{F}$ and $\overline{\rho f'}$ have the same type of variation throughout the flow field, nor to assess whether or not the correlation is always negligible.

To sum up, it is clear that, both theoretically and physically, the actual effects of the d.f.c. terms are not yet completely understood nor correctly modelled if necessary. The aim of this paper is to improve the understanding of the effects of d.f.c. terms by analysing their influence on the global behaviour and second-order properties of inhomogeneous jets and scrutinizing the d.f.c. effects on second-order modelling of variable-density turbulent mixing.

The core of the paper is split into six sections. In the next one, the origin of the various d.f.c. tems is analysed as a consequence of the nonlinearities of the mixing-driven variable-density situation. A brief survey of three different procedures for tackling the d.f.c. terms in the open set of equations is given in § 3. The second-order modelled set of equations is described in § 4. The numerical predictions are

compared with the experimental data for both the constant-density air jet and a CO_2–air jet in § 5. In § 6, density effects are examined by considering two predicted light jet flows. Then the influence of the d.f.c. terms on the global physical behaviour of inhomogeneous jets and on the predictions based on second-order modelling is discussed. Concluding remarks are given in § 7.

2. Analytical analysis of the nonlinearities of the free mixing-driven variable-density flow

As mentioned in the introduction, any statistical averaging of the local variable-density equations raises the problem of the analysis and the interpretation of the correlation terms deriving from the nonlinearities associated with the density. We shall now detail these nonlinear terms and the corresponding d.f.c., by considering first the equation of state, then the mean equations of motion.

2.1. *The equation of state*

Let us consider the mixing of two non-reactive gases at the same pressure and temperature. The equation of state reduces to

$$\frac{1}{\rho} = \frac{C}{\rho_1} + \frac{1-C}{\rho_2}, \tag{2.1}$$

where C stands for the mass fraction of one species (say 1). The densities of the two pure species are ρ_1 and ρ_2. Equation (2.1) is equivalent to

$$\rho = a\rho C + b, \tag{2.2}$$

where $a = (\rho_1 - \rho_2)/\rho_1$ and $b = \rho_2$. Using the inlet density ratio $S = (\rho_{jet}/\rho_\infty)_0$, it can be seen that $a = 1 - 1/S$ for a pure gas $(\rho_{jet})_0 = \rho_1$ at the exit.

Introducing $C = \bar{C} + \gamma'$ with $\overline{\gamma'} = 0$, it is obtained from (2.2) that

$$\bar{\rho} + \rho' = a\left(\bar{\rho}\bar{C} + \rho'\bar{C} + \rho\gamma'\right) + b, \tag{2.3}$$

from which it results that

$$\bar{\rho} = a\left(\bar{\rho}\bar{C} + \overline{\rho\gamma'}\right) + b, \tag{2.4a}$$

$$\rho' = a\left(\rho'\bar{C} + \rho\gamma' - \overline{\rho\gamma'}\right). \tag{2.4b}$$

Let f' be the centred fluctuation ($\overline{f'} = 0$) of any scalar function F or velocity component; one can easily deduce from (2.4*b*) that

$$\overline{\rho' f'} \equiv \overline{\rho f'} = \frac{a}{1 - a\bar{C}}\,\overline{\rho\gamma' f'}. \tag{2.5}$$

Thus, when the mean mass fraction $\bar{C}$ is given, the $\overline{\rho f'}$ d.f.c. term is *exactly* linked to a second-order mass-weighted correlation so that $\overline{\rho f'}$ and $\overline{\rho f'\gamma'}$ cannot be considered as independent variables. As a straightforward application of (2.5), one gets respectively, for the density–velocity and the density–mass fraction correlations

$$\overline{\rho u_i'} = \frac{a}{1 - a\bar{C}}\,\overline{\rho\gamma' u_i'}, \tag{2.6a}$$

$$\overline{\rho\gamma'} = \frac{a}{1 - a\bar{C}}\,\overline{\rho\gamma'^2}. \tag{2.6b}$$

2.2. *The mean motion equations*

Let us first consider the continuity equation

$$\frac{\partial \rho}{\partial t} + \frac{\partial \rho U_j}{\partial x_j} = 0. \tag{2.7}$$

Introducing $U_i = \bar{U}_i + u_i'$ and $\rho = \bar{\rho} + \rho'$, with $\overline{u_i'} = \overline{\rho'} = 0$, the nonlinear term gives

$$\overline{\rho U_j} = \underbrace{\bar{\rho}\bar{U}_j}_{(a)} + \underbrace{\overline{\rho u_j'}}_{(b)}, \tag{2.8}$$

where, in addition to the mean contribution (a), a turbulent mass flux (b) is added, compared with the constant-density case. Turning now to the transport equation of any scalar property F, the nonlinearities are mostly concentrated in the triple product of the convective term:

$$\bar{A}_j(F) \equiv \overline{\rho F U_j} = \underbrace{\bar{\rho}\bar{F}\bar{U}_j}_{(a)} + \underbrace{\bar{\rho}\,\overline{f u_j'}}_{(b)} + \underbrace{\underbrace{\overline{\rho' f' u_j'}}_{(c_1)} + \underbrace{\overline{\rho' f'}\bar{U}_j + \overline{\rho' u_j'}\bar{F}}_{(c_2)}}_{(c)}. \tag{2.9}$$

In comparison with the constant-density situation where only the (a) and (b) contributions are present, three new additive correlations (c) appear in (2.9), a triple-order one (c_1) and two d.f.c. (c_2) ones.

3. The regrouping procedures and the associated interpretations of the first-order d.f.c. terms

When the density changes, as opposed to the constant-density situation, the formulation of the statistically averaged open equations is not evident nor unique. In fact, it depends on a *regrouping* procedure which is intimately connected with the physical interpretation of the additional density correlation terms. Among the various existing proposals, we shall only discuss here those of Favre (1958), Chassaing (1985) and Shih *et al.* (1987).

3.1. *The binary regrouping*

As far back as 1958, Favre introduced and generalized the so-called mass-weighted averaging, which basically consists in grouping any d.f.c. term into a *new* macroscopic mean value as, for instance, $\bar{\rho}\bar{U}_i$ and $\overline{\rho u_i'}$

$$\tilde{U}_i = \frac{\bar{\rho}\bar{U}_i + \overline{\rho u_i'}}{\bar{\rho}} \equiv \bar{U}_i + \frac{\overline{\rho u_i'}}{\bar{\rho}}. \tag{3.1}$$

Hence, introducing $U_i = \tilde{U}_i + u_i$, (2.8) is simply $\overline{\rho U_i} = \bar{\rho}\tilde{U}_i$, and (2.9) is reduced to a *binary regrouping* :

$$\bar{A}_j(F) = \bar{\rho}\tilde{F}\tilde{U}_j + \overline{\rho f u_j}, \tag{3.2}$$

where f denotes the fluctuation of F with respect to Favre's average. Formally, (3.2) includes no more nonlinear terms than for constant-density fluid motion. Such an analogy results from a physical argument, i.e. the macroscopic or mean conservation of mass in both cases. However, the 'mean' velocities of the constant- and variable-density flows are not defined in the same way, and consequently such kinematic

properties as the mean strain rate, the mean vorticity etc., are not physically identical in both cases. Finally, the Favrian fluctuation is not centred:

$$\tilde{f} = -\overline{\rho f'}/\bar{\rho}. \tag{3.3}$$

Thus, the formal incompressible analogy does not strictly apply to open second-order-moment transport equations, as shown for instance in Chassaing (1979).

3.2. *The ternary regrouping*

An alternative to the previous method, Chassaing (1985), consists in taking apart the d.f.c. terms and introducing the instantaneous value of the density into triple- (and higher) order density correlations leading to Reynolds' fluctuations mass-weighted second- (and higher) order moments. Consequently, a *ternary regrouping* is obtained in (2.9) by adding the (c_1) contribution to (b) to give

$$\bar{A}_j(F) = \underbrace{\bar{\rho}\bar{F}\bar{U}_j}_{(a)} + \underbrace{\overline{\rho f' u_j'}}_{(b')} + \underbrace{\overline{\rho f'}\bar{U}_j + \overline{\rho u_j'}\bar{F}}_{(c_2)}. \tag{3.4}$$

In (3.4), the (b') term is the 'compressible' or 'variable-density' equivalent to the classical second-order correlation and an open transport equation for this term can be exactly derived (Chassaing 1985). Owing to relations (2.6*a*) and (2.6*b*), all d.f.c. terms in (c_2) are not extra independent unknowns.

3.3. *The Shih et al. (S.L.J.) approximation*

The previous formulations were concerned with the divergence form of the instantaneous balance equations. Starting from the advective (transport) form of these equations, and dividing both sides by the density, it is noted that the convective nonlinearity is of exactly the same type as for the constant-density situation. When averaging, the problem is now to get tractable expressions for terms including $1/\rho$. Assuming that the density flucuation ρ' is of the order of its r.m.s. value ρ'', Shih *et al.* (1987) simplify the problem by noticing that relative density fluctuations $\rho''/\bar{\rho}$ are generally low. Thus, using a first-order approximation to $1/\rho$, the following obtained, using the notation of the present study:

$$\bar{\rho} = \frac{b}{1 - a\bar{C}} + O_1\left(\rho''\right)^2, \tag{3.5a}$$

$$\frac{\rho'}{\bar{\rho}} = \frac{a}{b}\bar{\rho}\gamma' + O_2\left(\frac{\rho''}{\bar{\rho}}\right)^2, \tag{3.5b}$$

from which it is deduced that the turbulent mass flux is approximated by

$$\overline{\rho u_j'} = \frac{a}{b}\bar{\rho}^2\overline{\gamma' u_j'} + O_3\left(\rho''\right)^3. \tag{3.6}$$

3.4. *Comments on the averaging procedures*

(*a*) As far as the open set of equations is concerned, the various formulations are obviously formally equivalent. For instance, from equations (2.4*a*) and (2.4*b*), the higher-order terms in (3.5*a*), (3.5*b*) and (3.6) can be obtained exactly (see Appendix A). Similarly, the relationship between the binary and ternary regrouping is detailed in Appendix B.

(*b*) Physically, Favre's analysis is partly based on a *mechanical interpretation* of the turbulent mass flux $\overline{\rho u_j'}$, since this term finds expression in a new macroscopic mean

velocity, independent of the physical origin of the density variation. By definition, the macroscopic evolution is mass conservative.

With the ternary regrouping, the kinematic properties do not change whether the density is constant or not. But, when the density varies, one has to deal with an open system analysis and some thermodynamic information is necessary to express the d.f.c. terms. According to this *thermodynamic linkage* the expressions for the $\overline{\rho f'}$ correlations depend on the law governing the density variation, as can be seen from Appendix C for a perfect gas law variation.

(*c*) Concerning the modelling procedure, two comments should be made:

(i) When dealing with second-order modelling and using Favre's averaging, one is concerned with the determination of $\bar{u}_i$ which appears explicitely in the open set of equations, see Chassaing (1979) for instance. This can be achieved by deriving and solving a modelled transport equation for $\bar{u}_i$, as proposed by Jones (1979) or developing a gradient-type submodel, as suggested by Driscoll *et al.* (1982). Such closing processes are not necessary with the ternary formulation.

(ii) Secondly, when elaborating single-point closure schemes with Favre's averaging, it is clear that the turbulent mass flux $\overline{\rho u_i'}$ – and more generally any d.f.c. term $\overline{\rho f'}$ – cannot be considered independently of the Reynolds' mean value $\bar{\rho}\bar{U}_i$ or $\bar{\rho}\bar{F}$ respectively. Let us consider now Sautet's measurements in a pure hydrogen–air jet ($S = 0.07$). The mean mass fraction $\bar{C}$, the non-dimensional d.f.c. term $\overline{\rho\gamma'}/\bar{\rho}$ and the mass fraction variance $\overline{\gamma'^2}$ profiles measured by Sautet at $x/D_0 = 12$ are plotted in figure 1(*a*). In figure 1(*b*), two second-order density–mass fraction correlations are shown: $\overline{\rho\gamma'^2}/\bar{\rho}$ which is deduced from (2.6), and $\overline{\rho'\gamma'^2}/\bar{\rho}$ which is obtained from

$$\overline{\rho\gamma'^2} \equiv \bar{\rho}\,\overline{\gamma'^2} + \overline{\rho'\gamma'^2}. \tag{3.7}$$

Two main observations emerge from figure 1

(i) the d.f.c. profile is quite different from that for mean mass-fraction;

(ii) all quantities have approximately the same orders of magnitude, except $(\overline{\rho\gamma'^2}/\bar{\rho})^{1/2}$ near the axis where the approximation $\overline{\rho\gamma'^2} \approx \bar{\rho}\,\overline{\gamma'^2}$ is justified.

According to the previous results and, as a provisional part of the conclusion, it can be said that, if it is always possible to convert Favre-averaged moments to Reynolds-averaged ones, there is no definitive reason to use mass-weighted averages, either from a theoretical, modelling or experimental point of view. In the present study, the ternary regrouping procedure is adopted and the following part of the paper is concerned with the analysis of density effects in jet flows, as a consequence of such a choice.

4. The modelled set of equations

The exact (open) transport equations for the mean values and second-order moments are given in Chassaing (1985) and will not be repeated here. Within the scope of this paper, the model and the associated numerical code are merely considered as means of carrying out comparative 'numerical experiments' restricted to extrapolating from satisfactorily well-predicted situations. Consequently, such questions as the generality of the closure schemes or the universality of the constants of the model are not discussed here. This also explains why such a refined model as proposed by Shih *et al.* (1987) is not necessary for the present study. The closure schemes were originally developed by Hérard (1986) based on turbulent invariant modelling techniques as done by Siess (1975). The result consists of (i) the extension of the conventional

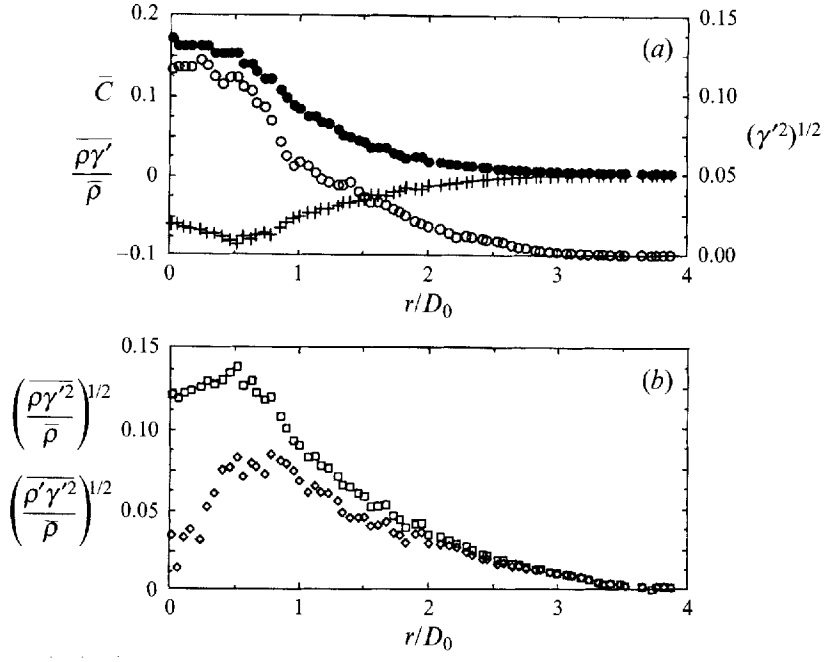

FIGURE 1. (*a*) •, Mean mass fraction ($\bar{C}$); +, first-order density–mass fraction correlation ($\overline{\rho\gamma'}/\bar{\rho}$); and ○, mean mass fraction variance $(\overline{\gamma'^2})^{1/2}$ in a pure hydrogen–air jet, from Sautet's measurements (1992). (*b*) Corresponding profiles of □, $(\overline{\rho\gamma'^2}/\bar{\rho})^{1/2}$ according to (2.6); and ◇, $(\overline{\rho'\gamma'^2}/\bar{\rho})^{1/2}$ according to (3.7).

models to mimic variable-density equivalents of constant density mechanisms, and (ii) the introduction of specific closure schemes to model the pressure correlation terms associated with the density fluctuations. Details on the second-order closure procedure can be found in Hérard (1986), Chassaing & Hérard (1987) and Chassaing & Chibat (1988). Only the final forms of the modelled equations are given here. The mean motion is steady, the turbulent Reynolds–Schmidt numbers are high enough and the molecular diffusion effects are neglected.

4.1. *The mean motion equations*

The mean continuity, momentum and mass fraction equations are

$$\frac{\partial \bar{\rho}\bar{U}_k}{\partial x_k} = -\frac{\partial \overline{\rho u_k'}}{\partial x_k}, \tag{4.1a}$$

$$\frac{\partial \bar{\rho}\bar{U}_i\bar{U}_k}{\partial x_k} + \frac{\partial}{\partial x_k}\left(\overline{\rho u_k'}\,\bar{U}_i + \overline{\rho u_i'}\,\bar{U}_k\right) = \bar{\rho}g_i - \frac{\partial \bar{P}}{\partial x_i} - \frac{\partial \overline{\rho u_i' u_k'}}{\partial x_k}, \tag{4.1b}$$

$$\frac{\partial \bar{\rho}\bar{C}\bar{U}_k}{\partial x_k} + \frac{\partial}{\partial x_k}\left(\overline{\rho u_k'}\,\bar{C} + \overline{\rho\gamma'}\,\bar{U}_k\right) = -\frac{\partial \overline{\rho\gamma' u_k'}}{\partial x_k}, \tag{4.1c}$$

where molecular effects are negligible with respect to the turbulent diffusion terms, according to the high turbulent Reynolds/Schmidt, numbers assumption. Thus (4.1*c*) is equivalent to

$$\frac{\partial}{\partial x_k}\left(\overline{\rho C U_k}\right) = 0.$$

Then, substituting the instantaneous value ρC from the equation of state (2.2), one finds

$$\frac{1}{a}\frac{\partial\overline{\rho U_k}}{\partial x_k} - \frac{b}{a}\frac{\partial\bar{U}_k}{\partial x_k} = 0.$$

Hence, due to (4.1a), it can be finally deduced that

$$\frac{\partial\bar{U}_k}{\partial x_k} = 0. \tag{4.2}$$

The turbulent mixing situation, as assumed here, is a divergence-free mean motion. This result can be used to enhance the difference between the two *mean* velocities $\bar{U}_i$ and $\tilde{U}_i$, since, with the same assumptions, $\partial\tilde{U}_k/\partial x_k = 0$ is no longer an exact equation.

4.2. *The second-order-moment transport equations*

Using the ternary regrouping, the double velocity $\overline{\rho u_i' u_j'}$, the double mass fraction $\overline{\rho\gamma'^2}$ and the velocity–mass fraction cross-correlations $\overline{\rho\gamma' u_j'}$ are taken as the main second-order unknowns. This means that these quantities are obtained by solving modelled transport equations. On the other hand, the d.f.c. terms are considered as linked variables, the values of which are given by the exact algebraic relations (2.6). Applying the mean divergence-free condition (4.2), the modelled equations are

Double velocity correlations:

$$\begin{aligned}\frac{\partial\left(\overline{\rho u_i' u_j'}\,\bar{U}_k\right)}{\partial x_k} = &-\left(\overline{\rho u_i'}\,\bar{U}_k\frac{\partial\bar{U}_j}{\partial x_k} + \overline{\rho u_j'}\,\bar{U}_k\frac{\partial\bar{U}_i}{\partial x_k}\right) + \bar{P}_{ij} + \left(\overline{\rho u_i' g_j} + \overline{\rho u_j' g_i}\right)\\ &+2A_0\bar{k}\bar{T}_{ij} - A_1\left(\bar{P}_{ij} - \tfrac{2}{3}\bar{Q}\delta_{ij}\right) - A_2\left(\bar{Q}_{ij} - \tfrac{2}{3}\bar{Q}\delta_{ij}\right) + A_3\bar{\varepsilon}\bar{b}_{ij}\\ &+A_4\left(\bar{U}_k\frac{\partial\bar{U}_l}{\partial x_k} - g_l\right)\left(\overline{\rho u_i'}\delta_{lj} + \overline{\rho u_j'}\delta_{li} - \tfrac{2}{3}\overline{\rho u_l'}\delta_{ij}\right)\\ &+D_1\frac{\partial}{\partial x_k}\left[\frac{\bar{k}}{\bar{\rho}\bar{\varepsilon}}\left(\overline{\rho u_k' u_l'} + \overline{\rho u_k'}\,\bar{U}_l\right)\frac{\partial\overline{\rho u_i' u_j'}}{\partial x_l}\right] - \tfrac{2}{3}\bar{\varepsilon}\delta_{ij}.\end{aligned} \tag{4.3}$$

In (4.3) the three terms on the right-hand side of the first line are exact. $\bar{k}$ is the mean turbulent kinetic energy ($\frac{1}{2}\overline{\rho u_i' u_i'}$) and $\bar{\varepsilon}$ the mechanical dissipation rate. As defined in Appendix D, $\bar{P}_{ij}$ and $\bar{Q}_{ij}$ are the production and the transposed production tensors, the common trace of which is $\bar{Q}$; $\bar{T}_{ij}$ is the mean strain rate tensor and $\bar{b}_{ij}$ is the anisotropic tensor.

Velocity–mass fraction cross-correlations:

$$\begin{aligned}\frac{\partial(\overline{\rho\gamma' u_i'}\,\bar{U}_k)}{\partial x_k} = &-\left(\overline{\rho u_i'}\,\bar{U}_k\frac{\partial\bar{C}}{\partial x_k} + \overline{\rho\gamma'}\,\bar{U}_k\frac{\partial\bar{U}_i}{\partial x_k}\right) + \bar{P}_{\gamma i} + \overline{\rho\gamma' g_i}\\ &+\frac{2}{3}(1-2B_0)\,\overline{\rho\gamma' u_k'}\frac{\partial\bar{U}_i}{\partial x_k} + 2B_0\overline{\rho\gamma' u_k'}\frac{\partial\bar{U}_k}{\partial x_i} - B_2\frac{\bar{\varepsilon}}{\bar{k}}\overline{\rho\gamma' u_i'}\\ &-\overline{\rho\gamma'}\left(B_1\bar{b}_{mi} + \frac{\delta_{mi}}{3}\right)\left(\bar{U}_k\frac{\partial\bar{U}_m}{\partial x_k} - g_m\right) + D_2\frac{\partial}{\partial x_k}\left(\frac{\bar{k}}{\bar{\varepsilon}}\overline{\rho u_k' u_l'}\,\frac{\partial\overline{\rho\gamma' u_i'}}{\bar{\rho}\,\partial x_l}\right).\end{aligned} \tag{4.4}$$

Double mass fraction correlation:

$$\frac{\partial(\overline{\rho\gamma'^2}\bar{U}_k)}{\partial x_k} = -2\overline{\rho\gamma'}\,\bar{U}_k\frac{\partial\bar{C}}{\partial x_k} - 2\overline{\rho\gamma' u_k'}\frac{\partial\bar{C}}{\partial x_k} + D_3\frac{\partial}{\partial x_k}\left(\frac{\bar{k}}{\bar{\varepsilon}}\frac{\overline{\rho u_k' u_l'}}{\bar{\rho}}\frac{\partial\overline{\rho\gamma'^2}}{\partial x_l}\right) - \bar{\varepsilon}_\gamma. \tag{4.5}$$

As before, the terms on the first line of the right-hand sides of (4.4) and (4.5) are exact, and the $\bar{P}_{\gamma i}$ vector is given in Appendix D. Moreover *exact* gravity terms appear in (4.3) and (4.4) as a direct consequence of the ternary regrouping on the modelling procedure.

4.3. *The equations of the dissipation rates*

To complete the closure, the mechanical and scalar dissipation rates $\bar{\varepsilon}$ and $\bar{\varepsilon}_\gamma$ are to be given. The mass fraction dissipation rate $\bar{\varepsilon}_\gamma$ is deduced from $\bar{\varepsilon}$ as suggested by Béguier, Dekeyser & Launder (1978):

$$\bar{\varepsilon}_\gamma = G\frac{\overline{\rho\gamma'^2}}{\bar{k}}\bar{\varepsilon},$$

where the constant G is taken equal to 1.7.

The mechanical dissipation rate $\bar{\varepsilon}$ is obtained by solving the following modelled transport equation:

$$\frac{\partial(\bar{\varepsilon}\bar{U}_l)}{\partial x_l} = -F_1\frac{\bar{\varepsilon}}{\bar{k}}\overline{\rho u_m'}\left(\bar{U}_l\frac{\partial\bar{U}_m}{\partial x_l} - g_m\right) - F_3\frac{\bar{\varepsilon}}{\bar{k}}\overline{\rho u_i' u_j'}\frac{\partial\bar{U}_i}{\partial x_j}$$
$$+F_5\frac{\partial}{\partial x_l}\left(\frac{\bar{k}}{\bar{\rho}\bar{\varepsilon}}\overline{\rho u_l' u_m'}\frac{\partial\bar{\varepsilon}}{\partial x_m}\right) - F_6\frac{\bar{\varepsilon}^2}{\bar{k}}. \tag{4.6}$$

4.4. *Values of the constants and the numerical procedure*

The values of the constants are given in table 1 and two points are emphasized here:

(*a*) the same values are used to predict the constant-density jet, the inhomogeneous heavy jet ($S > 1$) and the inhomogeneous light jet ($0 < S < 1$);

(*b*) the values are validated by comparison with experimental data for *both* the constant-density and the heavy-jet flow situations (§ 5).

Assuming parabolic (Prandtl) conditions, a numerical solver has been developed using the finite-volume technique of Patankar & Spalding (1970). Details on the different versions of the program can be found in Chassaing (1979) and Harran (1994). Also given in these references are various numerical checks including the sensitivity to inlet conditions and grid mesh size. Regarding the constants of the models, the two following points should be mentioned: (i) the same code is used to predict the three types of jet and (ii) the same kind of inlet conditions is prescribed for the three cases and corresponds to a fully developed constant-density pipe flow.

5. The comparison with experimental data

Before applying the model described above to the analysis of the d.f.c. effects, the numerical predictions should be compared with selected available experimental data. This point is addressed in the present section.

5.1. *The test flow configurations*

Two flow configurations will be used which consist of a free turbulent round jet discharging vertically into a quiescent atmosphere without stratification. The first one

Term	$\overline{\rho u_i' u_j'}$	$\overline{\rho\gamma' u_i'}$	$\overline{\rho\gamma'^2}$	$\bar{\varepsilon}$
Pressure correlation	$A_0 = -0.16$ $A_1 = 0.76$ $A_2 = 0.08$ $A_3 = -2.80$ $A_4 = 0.21$	$B_0 = -0.1$ $B_1 = 0$ $B_2 = 6.0$		$F_1 = 0.50$ $F_3 = 1.44$ $F_5 = 0.19$ $F_6 = 1.92$
Diffusion	$D_1 = 0.21$	$D_2 = 0.15$	$D_3 = 0.20$	

TABLE 1. Constants of the model

Case	Fluid	$\rho_0\,(\mathrm{kg\,m^{-3}})$	$\nu_0\,(\mathrm{m^2\,s^{-1}})$	S	$U_0\,(\mathrm{m\,s^{-1}})$	D_0(cm)	R_{e0}	F_{r0}
[*i*]	Air	1.21	15×10^{-6}	1	20.3	4	54100	–
[*h*]	80% CO_2 20% Air	1.73	8.6×10^{-6}	1.43	13.0	3.6	54400	1110

TABLE 2. Inlet parameters of the jet test flows.

[*i*] corresponds to $S = 1$ (constant-density flow) and the second one [*h*] to a heavy jet discharging vertically downwards. The values of the main significant parameters are given in table 2, where U_0 stands for the mean pipe flow exit velocity along the axis. The Reynolds and Froude numbers are respectively defined as $R_{e0} = U_0 D_0/\nu_0$ and $F_{r0}^{-1} = (S-1)\,gD_0/U_0^2$ As already mentioned, the jet exit conditions correspond to a fully developed pipe flow. In particular, the turbulent intensities are not uniform across the section, and the centreline values are not zero ($\overline{u'^2}/U_0^2 \approx \overline{v'^2}/U_0^2 \approx \overline{w'^2}/U_0^2 \approx 11\%$ for the constant-density jet). When available, the measured profiles are directly used to prescribe the inlet distributions for the numerical procedure. This can be done for the mean axial velocity, the mean mass fraction and the four significant Reynolds stresses. For more details on the measurement techniques, see Chassaing (1979)(referred to as C79 in figure captions). Finally, for the variable-density jet flow predictions, all the d.f.c. terms have been set equal to zero in the inlet section, that is $(\overline{\rho\gamma'})_0 = (\overline{\rho u'})_0 = (\overline{\rho v'})_0 = (\overline{\rho\gamma'^2})_0 = (\overline{\rho\gamma' u'})_0 = (\overline{\rho\gamma' v'})_0 = 0$.

5.2. *The constant-density jet*

5.2.1. *Streamwise variations*

Let us first examine the jet spreading rate as measured by the streamwise variation of the half-width velocity $\delta_{U_{0.5}}$. As pointed out by Launder & Morse (1977) this is a good test for second-order closure predictions in axisymmetric flows. As shown in figure 2, the agreement between the experimental data and the numerical results is good, in particular near the exit. As pointed out by Ha Minh & Chassaing (1978), this region is very crucial, since the flow has to restructure its characteristics from a fully developed pipe situation at the exit, to a free self-similar jet motion far downstream.

The computed value of the spreading rate in the linear region ($x/R_0 \geqslant 20$) is found to be equal to 0.09. It is in good agreement with the present pipe jet measurements and other values in the literature which refer to nozzle jets: 0.090 (Corrsin & Uberoi 1949), 0.082 to 0.091 (Florent 1966), 0.089 (Bradbury 1967), 0.084 (Wygnanski & Fiedler 1969), 0.085 (Schlünder 1971), 0.086 and 0.090 (Rodi 1972), 0.096 (Panchapakesan & Lumley 1993*a*). The same observations as before can be made for the variation of

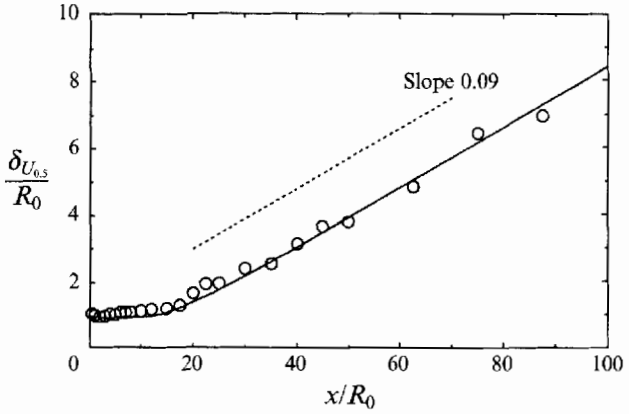

FIGURE 2. Constant-density jet: streamwise variation of half-width velocity $\delta_{U_{0.5}}$: ○, Exp. C79; —, model.

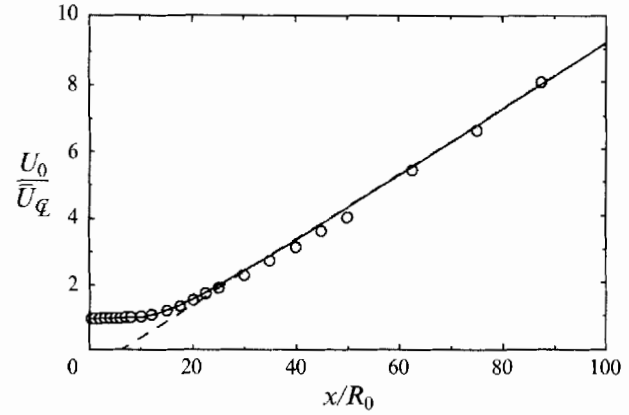

FIGURE 3. Constant-density jet: variation of mean centreline velocity $\bar{U}_{\mathcal{L}}$ along the jet axis. ○, Exp. C79; —, model; – – $\bar{U}_{\mathcal{L}}/U_0 = 5.15D_0/(x - 2.8D_0)$.

the mean axial velocity along the jet axis (figure 3). The restructuring of the flow is correctly predicted near the exit and the hyperbolic decrease of the centreline velocity is found to occcur at about the same location as the linear spreading rate of the jet ($x/R_0 = 20$).

In this region ($x/R_0 \geqslant 20$), the predicted law is $\bar{U}_{\mathcal{L}}/U_0 = 5.15D_0/(x - x^*)$, where the virtual origin is located at about $x^* \approx 2.8D_0$. The value of the coefficient, 5.15, is slightly lower than those given in the literature: 5.4 (Wygnanski & Fiedler 1969), 5.85 (Rodi 1972), 5.90 (Bogulawski & Popiel 1979), 6.06 (Panchapakesan & Lumley 1993*a*). However the agreement with the present pipe jet measurements is still satisfactory.

The last streamwise variation to be discussed is the turbulent kinetic energy $\bar{e} = \overline{u_i u_i}/2$ (figure 4). When normalized by the inlet velocity U_0, the turbulent kinetic energy reaches a maximum at about $x = 18R_0$. When normalized by the local centreline value of the mean velocity $\bar{U}_{\mathcal{L}}(x)$ the turbulent kinetic energy should reach a constant level according to self-similarity conditions. For nozzle jets, this seems to be achieved

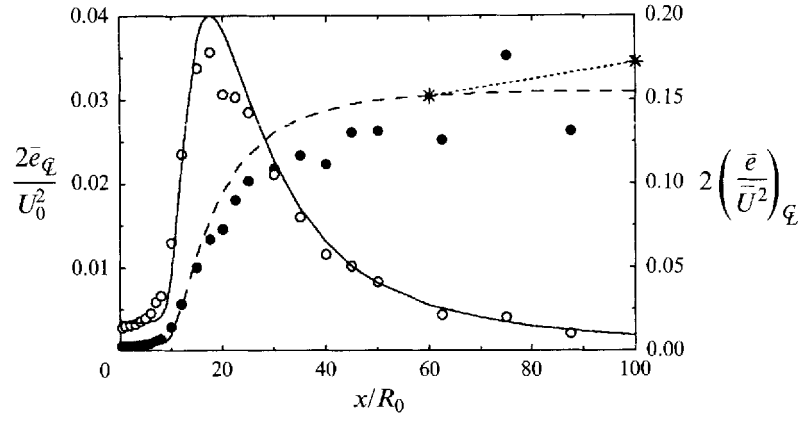

FIGURE 4. Constant-density jet: turbulent kinetic energy along the jet axis. $2\bar{e}_{\mathcal{L}}/U_0^2$: ○, Exp. C79; — , model. $2(\bar{e}/\bar{U}^2)_{\mathcal{L}}$: •, Exp. C79; – – , model; *, Wygnanski & Fiedler (1969).

at $x = 150R_0$ (Wygnanski & Fiedler 1969) and $x = 140R_0$ (Panchapakesan & Lumley 1993*a*). However, it is quite plausible that the measured value depends on the exit conditions and is different for the pipe jet configuration, as shown in figure 4. When comparing the predictions with the measurements of the pipe jet flow, it appears that the computed level ($2\bar{e}_{\mathcal{L}}/\bar{U}_{\mathcal{L}}^2 \approx 0.15$) is fairly constant for $60 \leqslant x/R_0 \leqslant 100$ and lies within the measurement range. It also agrees with the Wygnanski & Fiedler (1969) data in the same region, as reported in the same figure.

5.2.2. *Profiles*

The non-dimensional mean axial velocity and turbulent shear stress profiles are given in figures 5 and 6 respectively. The various profiles are presented for two different downstream locations: the first one ($x = 20R_0$) is located near the cross-section where the turbulent kinetic energy along the axis is maximum ($x = 18R_0$); the second one corresponds to the far-field part of the investigated region ($50R_0 \leqslant x \leqslant 100R_0$). To get non-dimensional quantities, the mean velocity at the exit (U_0) is used in order to make the comparison between the predictions and the measurements more relevant.

For the mean axial velocity, the agreement between experimental data and numerical results is satisfactory, except in the outer part of the jet where the classical hot-wire measurements are questionable due to high intermittency levels. Thus in Chassaing (1979), the exploration of the jet cross-sections was limited to a radial distance $r/x \approx 0.17$ as compared with 0.25 for the recent investigation of Panchapakesan & Lumley (1993*a*). The same comments also apply to the turbulent shear stress (figure 6).

When normalized by the centreline velocity, it can be easily demonstrated that

$$\text{when } r \to 0, \quad \frac{\overline{u'v'}}{\bar{U}_{\mathcal{L}}^2} \sim \frac{1}{2}\frac{r}{x} \tag{5.1}$$

as a direct consequence of the mean axial velocity self-similarity. At $x = 50R_0$, the measured value of this slope is close to 0.5. The same result was found by Panchapakesan & Lumley (1993*a*) for $120 \leqslant x/R_0 \leqslant 240$. Thus for the pipe jet, it seems that condition (5.1) is satisfied closer to the jet exit.

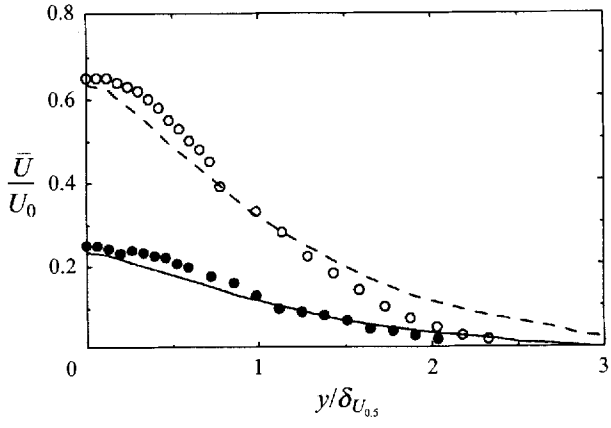

FIGURE 5. Constant-density jet: axial mean velocity profiles across the jet. $x/R_0 = 20$: ○, Exp. C79; – –, model. $x/R_0 = 50$: •, Exp. C79; —, model.

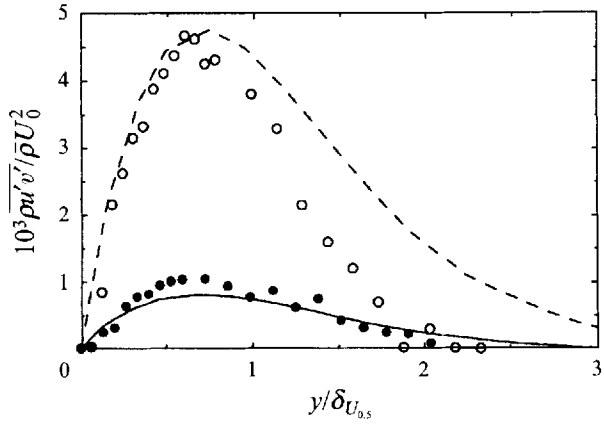

FIGURE 6. Constant-density jet: turbulent shear stress variation across the jet. Same symbols as in figure 5.

To summarize for the constant-density pipe jet flow, it can be said that: (i) the numerical results are in fairly good agreement with the measurements for both mean values and second-order moments, (ii) the restructuring of the flow is satisfactorily well predicted, (iii) the values of the jet spreading rate, the mean velocity centreline decay rate and the turbulent kinetic energy level in the self-similar region are close to those given in the literature, but not quite identical. The last conclusion was pointed out by Rodi (1972) who found that the centreline decay rate can be modified by 20% when changing the inlet velocity profile from a uniform distribution to that of a fully developed pipe flow. Similarly, the turbulent kinetic energy level can be changed by 60% if the inlet turbulent intensity varies from 0 to 4.4%. This explains why, in the numerical procedure, the inlet conditions are to be carefully prescribed as close as possible to the experimental data.

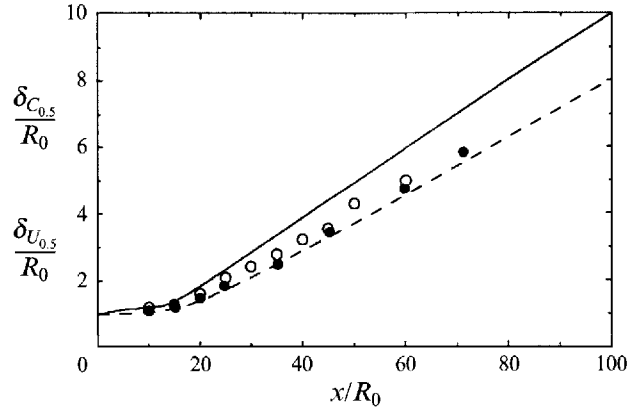

FIGURE 7. Heavy jet: streamwise variations of half-width velocity and mass fraction. $\delta_{C_{0.5}}/R_0$: ○, Exp. C79; —, model. $\delta_{U_{0.5}}/R_0$: •, Exp. C79; – –, model.

5.3. *The inhomogeneous heavy jet*

The 80% CO_2–20% air volume fraction (86% mass fraction) jet is now considered with a twofold purpose: (i) to serve as a second check of the model and numerical procedure, and (ii) to point out density effects associated with $S > 1$. We shall first discuss the mean and second-order-moment properties (streamwise variations and radial profiles), then the d.f.c. terms.

5.3.1. *Streamwise variations and jet spreading rates*

The streamwise variations of the half-width velocity ($\delta_{U_{0.5}}$) and mass-fraction ($\delta_{C_{0.5}}$) are given in figure 7. As for the constant-density situation, a linear variation is observed for $x \geqslant 20R_0$.

The dynamical velocity spreading rate, based on the slope of the half-width velocity is 0.087, very close to the one previously found (0.090) for the constant-density air jet. The slope of the linear variation of the mass-fraction radius $\delta_{C_{0.5}}$ is 18% higher (0.103) and is basically a consequence of the different curvatures of the mean-velocity and mass-fraction profiles. The virtual origins are also different and respectively equal to $3.8D_0$ and D_0 for the mean velocity and mass fraction.

The mean axial velocity and mass fraction along the axis, normalized by the exit values ($U_0/\overline{U}_{\mathcal{L}}$ and $C_0/\overline{C}_{\mathcal{L}}$ respectively) are given in figure 8. Owing to gravity effects, no rigourous self-similarity can be achieved. This point will be discussed later on (§ 6.1). However, for $x \geqslant 20R_0$, roughly hyperbolic centreline decay rates are observed according to

$$\frac{\bar{U}_{\mathcal{L}}}{U_0} \approx A\frac{D_0}{x - 1.35D_0}, \qquad \frac{\bar{C}_{\mathcal{L}}}{C_0} \approx B\frac{D_0}{x - 3D_0}, \tag{5.2}$$

with $A \approx 7.3$ and $B \approx 5.7$.

In order to compare these numerical values with the coefficients of the constant-density jet, Thring & Newby (1953) introduced an effective or equivalent diameter D_e such as $D_e = S^{1/2}D_0$, where it is recalled that S stands for the inlet density ratio $(\rho_{jet}/\rho_\infty)_0$. The corresponding values for the present study are then equal to $A_e \approx 6.1$ and $B_e = 4.8$. As reported by Sahr (1990) and corroborated by the reviews of Chassaing (1979) and Sautet (1992), the density effect is reduced but not suppressed by using an effective diameter such as that. In fact, from a wide literature survey (see

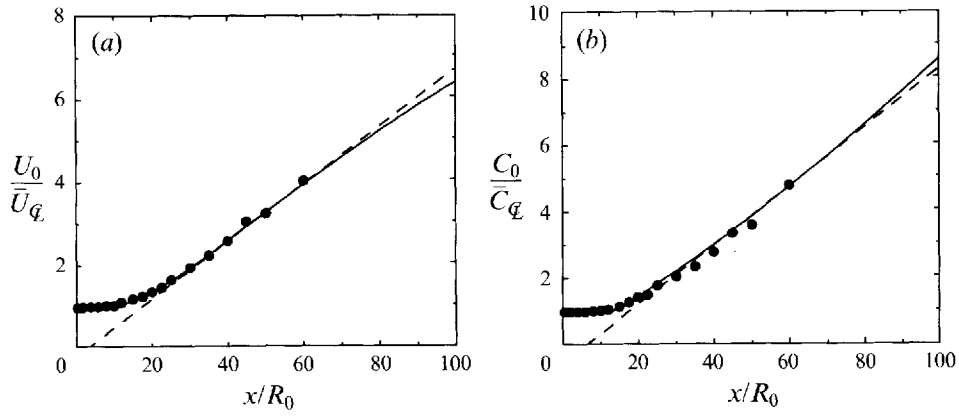

FIGURE 8. Heavy jet: (*a*) mean axial velocity and (*b*) mean mass fraction along the jet axis: •, Exp. C79; —, model; – –, equation (5.2).

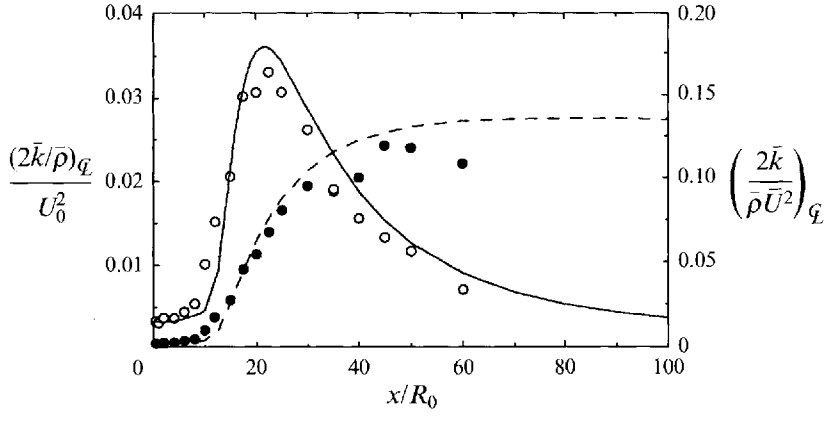

FIGURE 9. Heavy jet: turbulent kinetic energy along the jet axis. Same symbols as in figure 4.

references in figure 14 below), the values of A_e and B_e are found to be within the rather wide ranges [4.7–10.0] and [1.7–6.9], respectively. Actually, if density effects modify, by the same scaling factor, both A_e and B_e, the ratio A_e/B_e should be more relevant. From the available data, the following values can be obtained: 1.4 (Corrsin & Uberoi 1949), 1.5 (O'Connor, Comfort & Cass 1966), 1.5 (Sautet 1992), compared with 1.3 for the present study.

The streamwise variation of the turbulent kinetic energy along the axis of the heavy jet is given in figure 9. When normalized by the local mean axial velocity $\bar{U}_{\mathcal{C}}$, the trend towards self-similarity is observed with a constant value of $(2\bar{k}/\bar{\rho}\,\bar{U}^2)_{\mathcal{C}}$ of about 13%, slightly lower than the value found for the constant-density jet (15%).When normalized by the inlet velocity U_0 the variation of this quantity is qualitatively similar to that of the constant-density jet. However, the downstream location of the maximum is not the same: $11.5D_0$ instead of $9D_0$ for the constant-density jet. The value measured by Sautet (1992) for a pure CO_2 jet is $12D_0$.

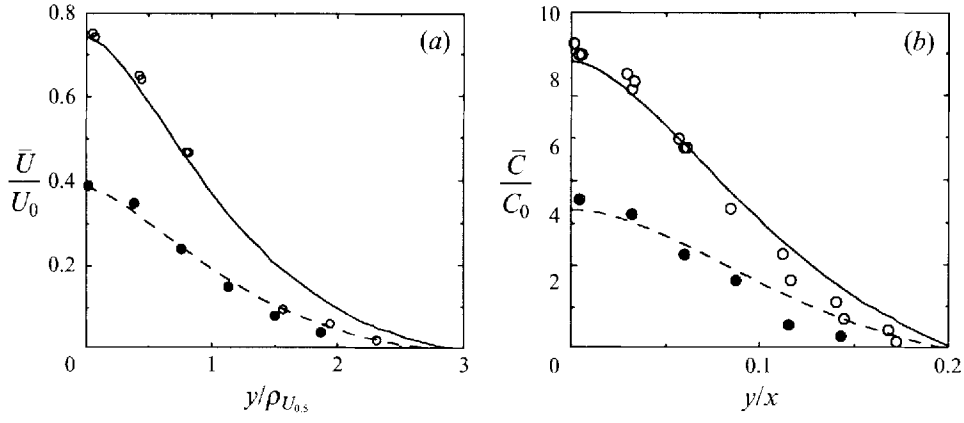

FIGURE 10. Heavy jet: (*a*) mean axial velocity and (*b*) mean mass-fraction profiles across the jet. $x/R_0 = 20$: ○, Exp. C79; —, model. $x/R_0 = 40$: •, Exp. C79; – –, model.

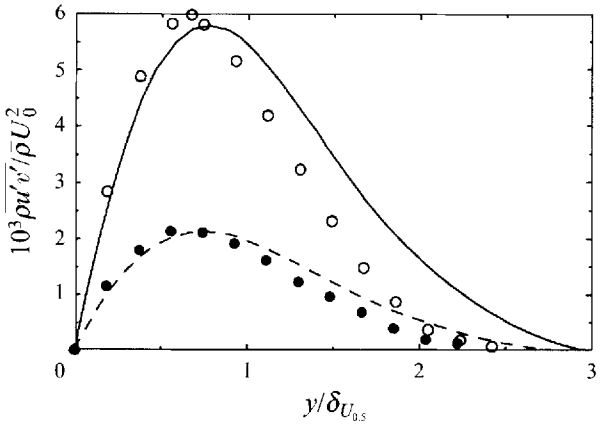

FIGURE 11. Heavy jet: turbulent shear stress profiles. Same symbols as in figure 10.

Finally it should be added that the predicted and measured values are not identical since the former, for instance, refer to $\overline{\rho u'^2}$, and the latter to $\overline{u'^2}$, as explained in Chassaing (1977). Nevertheless, the difference $\overline{\rho u'^2} - \bar{\rho}\overline{u'^2} \equiv \overline{\rho' u'^2}$ is not likely to introduce significant discrepancies owing to the moderate value of the inlet density ratio of the present study. In fact, it has been checked that the difference between $\overline{\rho u_i' u_j'}$ and $\bar{\rho}\,\overline{u_i' u_j'}$ was less than 1%, so that the approximate expression can be used for the comparison with the measurements.

5.3.2. *Mean and second-order-moment profiles*

The mean velocity and mass-fraction profiles are given in figure 10. As for the constant-density jet, the agreement between measurements and predictions can be considered as satisfactory, except in the outer part of the flow field. The same conclusion is also true for the turbulent shear stress as shown in figure 11.

Case	$\rho_0(\mathrm{kg\,m^3})$	$\nu_0(\mathrm{m^2\,s^{-1}})$	S	$U_0(\mathrm{m\,s^{-1}})$	D_0(cm)	R_{e0}	F_{r0}
$[l_1]$	0.85	21×10^6	0.70	31.8	3.6	54 100	−9 545
$[l_2]$	0.69	26×10^6	0.57	39.2	3.6	54 400	−10 120

TABLE 3. Inlet parameters of the light jets.

Case	$[h]$	$[i]$	$[l_1]$	$[l_2]$
S	1.43	1.0	0.70	0.57
$\delta_{U_{0.5}}/x - x_U^*$	0.087	0.09	0.094	0.096
x_U^*/D_0	3.8	3.0	4.0	4.4
$\delta_{C_{0.5}}/x - x_C^*$	0.103	–	0.118	0.123
x_C^*/D_0	1.0	–	2.2	2.5

TABLE 4. Influence of the density ratio on the jet spread.

5.3.3. *D.f.c. terms*

The computed spatial distributions of $\overline{\rho u'}/\bar{\rho}$ and $\overline{\rho\gamma'}/\bar{\rho}$ are illustrated in figure 12. Since all these d.f.c. terms are zero in the inlet section, several observations emerge when comparing with the corresponding $\bar{U}$ and $\bar{C}$ mean values distributions:

(i) the d.f.c. terms are positive everywhere;

(ii) the orders of magnitude are different, with approximatively $O(\bar{\rho}\bar{U}) > 200 \times O(\overline{\rho u'})$ and $O(\bar{\rho}\bar{C}) > 50 \times O(\overline{\rho\gamma'})$;

(iii) near the exit ($x/D_0 < 20$), the spanwise distributions of the d.f.c. terms and the mean values are clearly different, since $\bar{U}$ and $\bar{C}$ are maximum along the axis and the d.f.c. terms are maximum near the edge of the jet;

(iv) further downstream, $\overline{\rho u'}/\bar{\rho}$ and $\overline{\rho\gamma'}/\bar{\rho}$ evolve in different ways. The turbulent mass flux is always close to zero along the axis, but the maximum of the mass fraction–density fluctuation correlation is located on the axis at about $x \approx 35D_0$.

6. Results and discussion

6.1. *The inhomogeneous light jets*

The above results on the influence of the density ratio on the jet properties for $S > 1$ need to be completed for the case $S < 1$. This is done by running the *same* numerical code, with the *same* values of the constants of the model and the *same* type of inlet profiles. Two light jet flows are introduced with the inlet parameters given in table 3. They correspond to fictitious fluids since the kinematic viscosities are taken equal to the dynamical viscosity of air divided by a density value corresponding to one of the two following situations. The first one $[l_1]$ is $S_{l_1} = 1/S_h$, where $S_h = 1.43$ is the value of the heavy jet. For the second one $[l_2]$, $S_{l_2} - 1 = -(S_h - 1)$, so that the density differences with air of the heavy jet and this light jet are opposite. As for the heavy jet, gravity acts in the same way as the mean momentum, that is the heavy jet is discharging vertically downwards, and the light jet vertically upwards. The Reynolds number is taken constant for both cases (54 100), but the Froude numbers are slightly different.

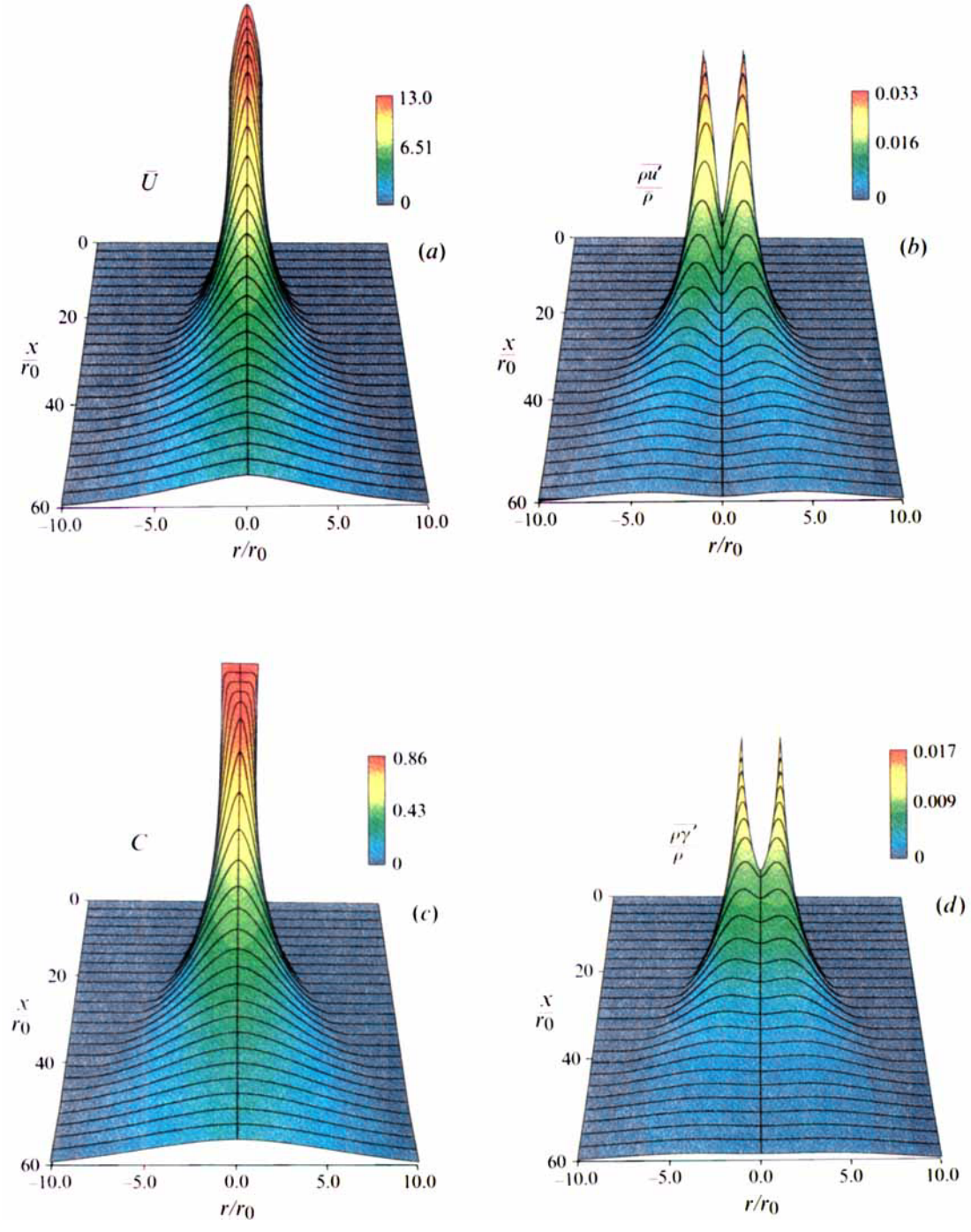

FIGURE 12. Heavy jet: (*a*) mean axial velocity, (*b*) density–velocity fluctuation correlation; (*c*) mean mass fraction, (*d*) density–mass fraction fluctuation correlation.

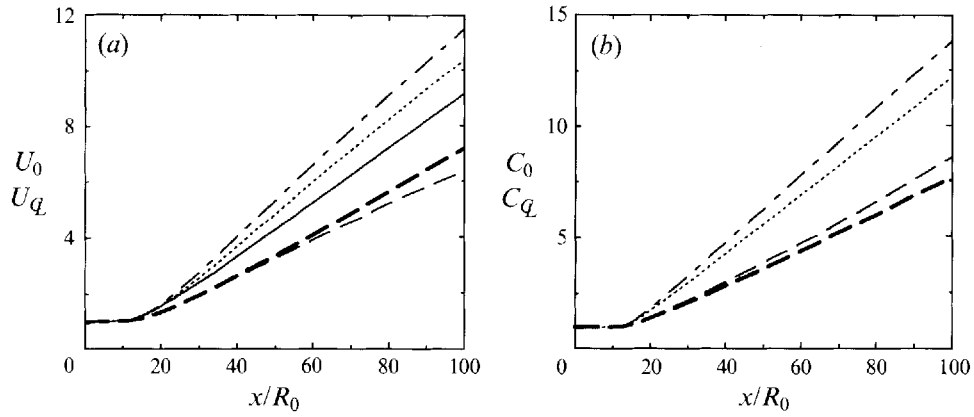

FIGURE 13. Decay of centreline mean velocity (*a*) and centerline mean mass-fraction (*b*) for different density ratios: – · –, $S = 0.57$; – – –, $S = 0.7$; ——, $S = 1.0$; – –, $S = 1.43$ and $g = 9.81\text{m s}^{-2}$; – –, $S = 1.43$ and $g = 0$.

6.1.1. *Streamwise variations and jet spreading rate*

As previously observed for the constant-density and heavy jets, the half-width velocity and mass-fraction thickness of the light jets exhibit linear variations for $x/R_0 > 20$. The corresponding values of the slopes and the virtual origins are given in table 4.

The jet spreading rates appear to be a slightly decreasing function of the density ratio. The sensitivity to S is more noticeable on the half-width mass fraction, which is changed by a factor of about 16%, compared with 9% for the velocity, over the present variation range of S. A different conclusion was reached by Richards & Pitts (1993) who reported that the mass-fraction spreading rate is identical over the range $0.138 \leqslant S \leqslant 1.552$. However, it should be pointed out that the present result could not be observed owing to the experimental uncertainty, which can be as high as $\pm 8\%$. Actually, and in qualitative agreement with Richards & Pitts (1993), it is the virtual origin which is most modified by the density ratio: 47% for the velocity, 150% for the mass fraction. This influence of the density ratio on the jet spreading rate is corroborated by the centreline decays of the mean velocity and mass fraction given in figure 13. In particular, the lack of symmetry with respect to the constant-density jet can be observed.

Before discussing the global differences in growth behaviour for the various variable-density jets, the question of the influence of buoyancy should be addressed.

(*a*) Buoyancy effects become important at different downstream positions for the heavy and light jets. Following Chen & Rodi (1976) for instance, the downstream extent of the inertial region of the jet is given by

$$\frac{X_{in}}{D_0} = 0.5\, S^{1/4}\, F_{r_0}^{1/2},$$

which corresponds to $X_{in} \approx 18D_0$, $45D_0$, $44D_0$ for the $[h]$, $[l_1]$ and $[l_2]$ cases respectively. Thus the heavy jet appears to be more sensitive to buoyancy effects than the light ones.

(*b*) The curvature in plots such as figure 13 ($S = 1.43$) are due to buoyancy effects. Focussing on the heavy jet, this can be readily shown by comparing the results of

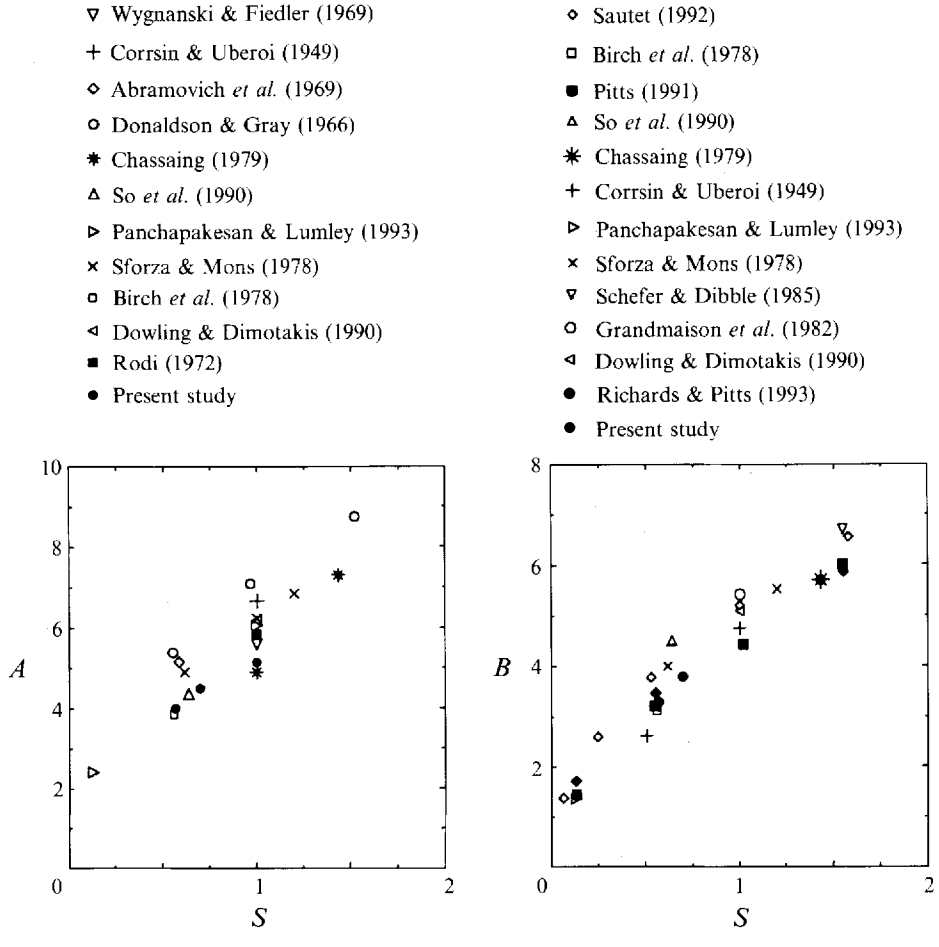

FIGURE 14. Centreline decay rates coefficients according to equations (5.2).

two computations: with and without gravity. When gravity is set equal to zero, a self-preservation state is achieved as shown by the linearity of the curves for $x/R_0 \geqslant 20$. However, it cannot be concluded from the present study whether zero-gravity variable-density jets achieve a *unique* self-preserving state or obey similarity conditions with different centreline decays and spreading rates (George 1989). Within the range $20 \leqslant x/R_0 \leqslant 100$, the centreline decay rates of mean velocity and mass fraction can be approximated by (5.2). The corresponding values of coefficients A and B are plotted in figure 14.

Since no equivalent diameter nor density is introduced here, an explicit comparison with the measurements of several authors is possible. As shown in the figure, the predicted values of B are in quite satisfactory agreement with the experimental data, for both heavy and light jets. The A coefficient is slightly lower than most of the values found in the literature. But, as noted for the constant-density jet, the reason is likely due to the specific exit conditions of the present study.

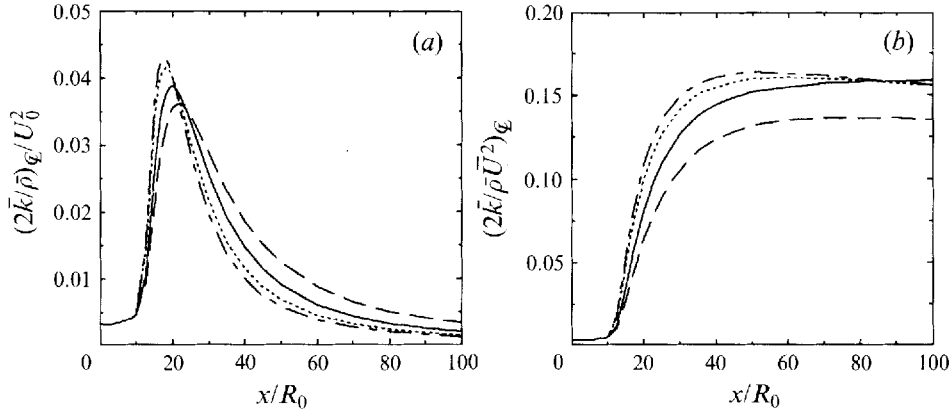

FIGURE 15. Turbulent kinetic energy along the jet axis for different inlet density ratios: (*a*) $2(\bar{k}/\bar{\rho})_{\mathcal{C}}/U_0^2$; (*b*) $2(\bar{k}/\bar{\rho}\,\bar{U}^2)_{\mathcal{C}}$. Same symbols as in figure 13.

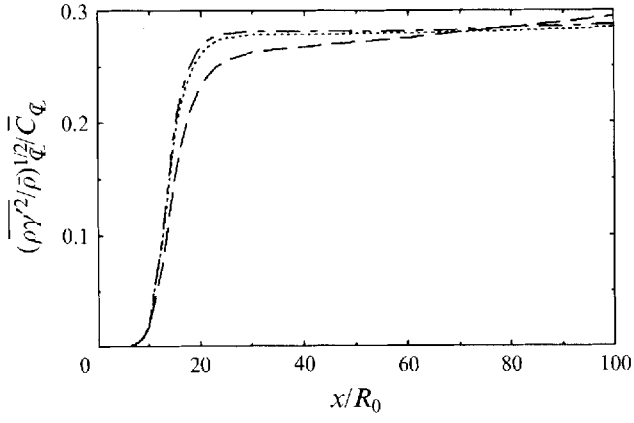

FIGURE 16. Mass-fraction variance $(\overline{\rho\gamma'^2}/\bar{\rho})_{\mathcal{C}}^{1/2}/\bar{C}_{\mathcal{C}}$ along the jet axis. Same symbols as in figure 13.

6.1.2. *Turbulent kinetic energy and mass-fraction variance*

The next quantity to be examined is the turbulent kinetic energy $\bar{k} = \overline{\rho u_i u_i}$ along the axis (figure 15). The same observations as before are confirmed, that is (i) the influence of S on both the value and the localization of the maximum of the turbulent kinetic energy along the axis, when normalized by the exit velocity U_0, and (ii) the trend towards a quasi-constant level, when normalized by the mean centreline velocity $\bar{U}_{\mathcal{C}}$. However, the growth curves corresponding to the light jets exhibit some kind of overshoot near $x = 40R_0$. A very similar result is observed for the variation of the mass-fraction variance $\overline{\rho\gamma'^2}$ along the axis, as given in figure 16.

6.1.3. *D.f.c terms*

Let us turn now to the velocity and mass-fraction density correlations, figures 17(*a*) and 17(*b*). Several points emerge:

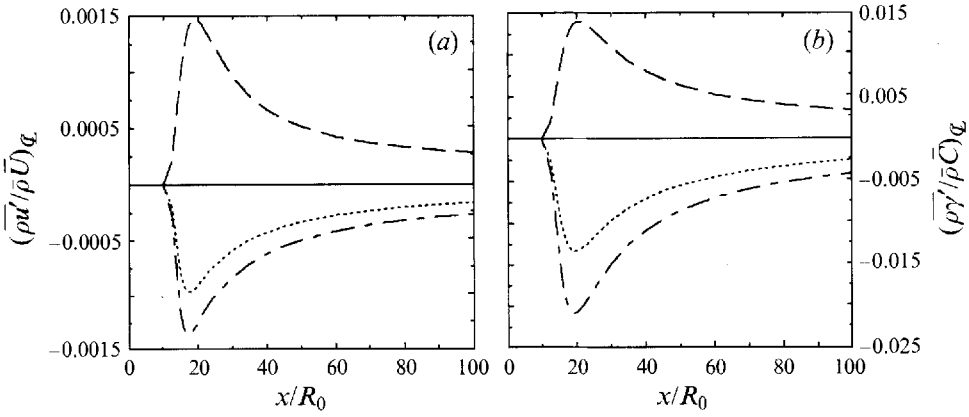

FIGURE 17. D.f.c. terms along the axis: (*a*) turbulent mass flux, (*b*) mass-fraction–density correlation. Same symbols as in figure 13.

(*a*) the sign of the d.f.c. terms changes, depending upon whether S is greater or lower than unity;

(*b*) both d.f.c. terms are positive for the heavy jet and negative for the light jets;

(*c*) when normalized by the respective centreline values, the absolute value of $\overline{\rho u'}/\bar{\rho}\bar{U}$ is approximately ten times lower than the absolute value of $\overline{\rho\gamma'}/\bar{\rho}\bar{C}$;

(*d*) the extrema of the d.f.c. terms along the axis are located near the downstream section where the turbulent kinetic energy is a maximum.

To the authors' knowledge, no measurements are available for direct comparison with the same jet flow. However, it can be mentioned that the results of So *et al.* (1990) for a light jet ($S = 0.64$) are in qualitatively good agreement with the predictions of the present study, although the Reynolds numbers are different (4300 and 54100 respectively). Quantitatively, the values in the far field also agree, but the predicted value of the extremum is nearly a factor of two lower than the measured one.

To sum up, it can be said that, despite the rather moderate departures from the constant-density case considered here, density effects can be observed on both heavy and light jets. These effects are not *symmetrical* with respect to the constant-density situation. D.f.c. terms are positive for the heavy jet ($S = 1.43$), and negative for the light jets ($S = 0.70$ and $S = 0.57$). Such a lack of symmetry was anticipated: for another reason, So & Liu (1986) noticed that the d.f.c. term was small for a jet fluid heavier than air, but non-negligible for a jet fluid lighter than air.

As just shown by the above results, the d.f.c. terms are significantly sensitive to the density ratio. We shall try now to explain such an observation and find out whether the sensitivity of the d.f.c. terms to the density ratio is qualitatively and quantitatively significant enough to account for some of the differences between the constant- and variable-density jet flows. The qualitative trends are first examined, based on analytical considerations, then the quantitative aspects are discussed (§6.9).

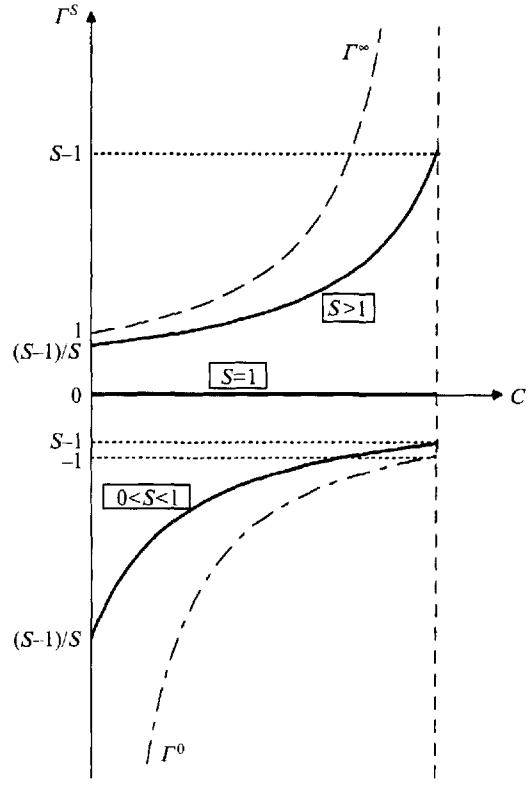

FIGURE 18. Γ^S variation versus the mean mass fraction $\bar{C}$: – –, $S = \infty$; – · –, $S = 0$.

6.2. *Influence of the density ratio on the density–mass fraction fluctuation correlation*

The first point to be explained is the change of the sign of the $\overline{\rho\gamma'}$ correlation with respect to S being greater or lower than unity. From (2.6) it is clear that

$$\frac{\overline{\rho\gamma'}}{\overline{\rho\gamma'^2}} = \frac{\overline{\rho u_i'}}{\overline{\rho\gamma' u_i'}} = \frac{S-1}{S-(S-1)\bar{C}} \equiv \Gamma^S(\bar{C}). \tag{6.1}$$

The variations of Γ^S versus the mean mass fraction $\bar{C}$ are sketched in figure 18 for $0 \leqslant \bar{C} \leqslant 1$.

Two major conclusions can be drawn:

(*a*) Γ^S is positive for $S > 1$, negative otherwise, and of course Γ^1 is identically zero;

(*b*) from (6.1), two asymptotic limits can be found for $\Gamma^S(\bar{C})$:

$$\text{when } S \to 0 \quad \Gamma^S(\bar{C}) \to \Gamma^0(\bar{C}) \approx \frac{-1}{\bar{C}}, \tag{6.2a}$$

$$\text{when } S \to +\infty \quad \Gamma^S(\bar{C}) \to \Gamma^\infty(\bar{C}) \approx \frac{1}{1-\bar{C}}. \tag{6.2b}$$

As a consequence of (*a*), it can be easily deduced from (6.1) that $\overline{\rho\gamma'}$ is positive when $S > 1$ and negative otherwise, since the $\overline{\rho\gamma'^2}$ correlation is always positive (the instantaneous values of ρ and γ'^2 are non-negative random functions). Then, from

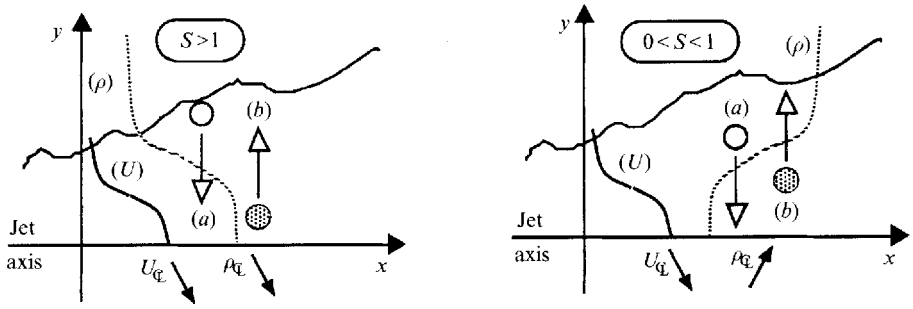

FIGURE 19. Sketch of the turbulent mixing in variable-density jets.

(3.5*b*) it is found that

$$\rho' = \frac{S-1}{bS}\bar{\rho}^2\gamma' + \bar{\rho}O_2\left(\frac{\rho''}{\bar{\rho}}\right)^2,$$

from which it is inferred that the density and mass-fraction fluctuations have the same sign when $S > 1$ and opposite signs otherwise. This result will be recalled in table 5.

Let us turn now to the consequences of (*b*) and notice first that, for a variable-density turbulent free jet, the overall shape of the mean mass-fraction profile is the same whether S is greater or lower than unity. Thus from (6.2*a*), it is deduced that in a light jet, the absolute value of the difference between the first- and second-order correlations is maximum near the outer edge of the flow. On the other hand as shown by (6.2*b*), this maximum is reached near the axis of a heavy jet, and is greater when the section is located near the exit.

In conclusion, it appears that, when the density ratio changes, both the signs and the spatial distributions of the density–mass fraction correlation terms are modified compared with the second-order mass-fraction moments.

6.3. *Signs of the velocity–density correlation terms in a free jet*

Let us examine now the signs of the turbulent mass fluxes $\overline{\rho u'}$ and $\overline{\rho v'}$. Like the measurements of Driscoll *et al.* (1982) in a turbulent non-premixed flame where $S = 0.36$, the correlations herein have been found negative when $0 < S < 1$. However they are positive when $S > 1$. From (6.1), this can be explained by a phenomenological analysis considering the two jet mixing situations sketched in figure 19. In such flows, it can be said that, at any given downstream location, the mixing occurs from fluid convected towards the axis (*a*) or towards the outer edge of the jet (*b*). On the average, when $S > 1$, the first case (*a*) corresponds to a negative density fluctuation, a negative axial velocity fluctuation and a negative radial velocity fluctuation. The four cases depicted in figure 19 can be analysed in the same way leading to the results given in table 5.

Three major conclusions can be drawn from table 5.

(*a*) The second-order moments are always positive. For the velocity correlations, this reinforces the fact that the $\overline{\rho u' v'}$ moment acts like the Reynolds shear stress of the constant-density jet flow.

(*b*) For a given value of S, all d.f.c. terms have the same sign.

(*c*) The d.f.c. terms are positive when $S > 1$ and negative otherwise. The signs of the

		ρ'	γ'	u'	v'	$\overline{\rho'\gamma'}$	$\overline{\rho'u'}$	$\overline{\rho'v'}$	$\overline{\rho\gamma' u'}$	$\overline{\rho\gamma' v'}$	$\overline{\rho u' v'}$
$S > 1$	(*a*)	−	−	−	−	+	+	+	+	+	+
	(*b*)	+	+	+	+	+	+	+	+	+	+
$0 < S < 1$	(*a*)	+	−	−	−	−	−	−	+	+	+
	(*b*)	−	+	+	+	−	−	−	+	+	+

TABLE 5. Signs of d.f.c. and second-order moments in a free turbulent inhomogeneous jet. Cases (*a*) and (*b*) are defined in figure 19.

d.f.c. terms are of major importance in explaining some basic qualitative differences between the global features of heavy and light jets as we shall see hereafter.

6.4. *The asymptotic forms of the continuity and mean mass-fraction equations*

Using the previous results, the mean continuity equation (4.1*a*) can be rewritten as follows:

$$\bar{U}_j \frac{\partial \bar{\rho}}{\partial x_j} = -\frac{\partial}{\partial x_j}\left(\Gamma^S \overline{\rho\gamma' u_j'}\right),$$

which leads to the asymptotic forms:

$$S \to 0 \;:\quad \bar{U}_j \frac{\partial \bar{\rho}}{\partial x_j} = \frac{\partial}{\partial x_j}\left(\frac{\overline{\rho\gamma' u_j'}}{\bar{C}}\right) \equiv \frac{1}{\bar{C}} \frac{\partial \overline{\rho\gamma' u_j'}}{\partial x_j} - \frac{\overline{\rho\gamma' u_j'}}{\bar{C}^2} \frac{\partial \bar{C}}{\partial x_j}, \tag{6.3a}$$

$$S \to +\infty \;:\; \bar{U}_j \frac{\partial \bar{\rho}}{\partial x_j} = -\frac{\partial}{\partial x_j}\left(\frac{\overline{\rho\gamma' u_j'}}{1-\bar{C}}\right) \equiv \frac{1}{\bar{C}-1} \frac{\partial \overline{\rho\gamma' u_j'}}{\partial x_j} - \frac{\overline{\rho\gamma' u_j'}}{(1-\bar{C})^2} \frac{\partial \bar{C}}{\partial x_j}. \tag{6.3b}$$

Thus in the mean continuity equation, the d.f.c. term has a double effect: (i) changing the coefficient of the turbulent mass-fraction diffusion term (asymptotically $1/\bar{C}$ and $1/(\bar{C}-1)$) and (ii) adding a mean mass-fraction gradient term which is always positive for two-dimensional free binary jets.

The mean mass-fraction transport equation can be treated in the same way. After some simple algebraic manipulations, and taking into account the mean divergence-free condition (4.2), the mean mass-fraction balance equation (4.1*c*) can be exactly rewritten as follows:

$$\left(\bar{\rho}\bar{U}_j + \overline{\rho u_j'}\right) \frac{\partial \bar{C}}{\partial x_j} = \underbrace{-\frac{\partial\left(\overline{\rho\gamma' u_j'}\right)}{\partial x_j}}_{(a)} \underbrace{-\bar{U}_j \frac{\partial}{\partial x_j}\left(\overline{\rho\gamma'}\right)}_{(b)}.$$

Compared with the constant-density case, where only the turbulent diffusion term (*a*) is present, the previous equation clearly shows that the d.f.c. term (*b*) on the right-hand side adds new contributions which have the following asymptotic expressions:

$$S \to 0 \;:\quad -\bar{U}_j \frac{\partial \overline{\rho\gamma'}}{\partial x_j} = \bar{U}_j \frac{\partial}{\partial x_j}\left(\frac{\overline{\rho\gamma'^2}}{\bar{C}}\right) \equiv \frac{\bar{U}_j}{\bar{C}} \frac{\partial \overline{\rho\gamma'^2}}{\partial x_j} - \frac{\overline{\rho\gamma'^2}}{\bar{C}^2} \bar{U}_j \frac{\partial \bar{C}}{\partial x_j}, \tag{6.4a}$$

$$S \to +\infty \;:\; -\bar{U}_j \frac{\partial \overline{\rho\gamma'}}{\partial x_j} = -\bar{U}_j \frac{\partial}{\partial x_j}\left(\frac{\overline{\rho\gamma'^2}}{1-\bar{C}}\right) \equiv \frac{\bar{U}_j}{\bar{C}-1} \frac{\partial \overline{\rho\gamma'^2}}{\partial x_j} - \frac{\overline{\rho\gamma'^2}}{(1-\bar{C})^2} \bar{U}_j \frac{\partial \bar{C}}{\partial x_j}. \tag{6.4b}$$

Qualitatively, the situation is thus quite similar to the one for the mean continuity equation (6.3).

6.5. *Influence of the density ratio on the centreline mean velocity decay rate*

As previously noticed (§ 5.3), an equivalent diameter is often introduced to account for density effects on the centreline decay rates of the mean mass fraction and axial velocity. However, when defined according to Thring & Newby (1953), the various measurements do not perfectly collapse when S changes. This is the reason why the definition of the effective diameter is modified to:

$$D_e = D_0 \left(S \frac{\rho_\infty}{\rho_e} \right)^{1/2}, \tag{6.5}$$

where ρ_e is an effective density. Several proposals have been made for this quantity by Pitts (1986), Stepowski *et al.* (1988), Sarh (1990), Sautet (1992) and Richards & Pitts (1993) for instance. The agreement is generally improved but, as we shall see now, the influence of S cannot be reduced to such a global formulation.

For a free turbulent round jet exhausting into a quiescent atmosphere without stratification, the mean momentum equation (4.1*b*) along the axis simplifies to:

$$\left(\bar{\rho} \bar{U} \frac{\partial \bar{U}}{\partial x} \right)_{\mathcal{L}} = - \left[\frac{1}{r} \frac{\partial}{\partial r} \left(r \overline{\rho u' v'} \right) \right]_{r=0} + (\bar{\rho} - \rho_\infty)_{\mathcal{L}} g_x - \bar{U}_{\mathcal{L}} \left(\frac{\partial \overline{\rho u'}}{\partial x} \right)_{r=0}, \tag{6.6}$$

where only the d.f.c. contribution to the mean advection term has been disregarded. Compared with the constant-density situation, where the centreline decay rate is entirely governed by the turbulent diffusion, two differences appear due to both gravity and d.f.c. terms. However, since the vertical directions of the heavy and light jets are inverted, the gravity forces always act in the same way in both cases ($S > 1$ or $0 < S < 1$). Hence, if the inlet density values of the light and heavy jets are such that the departures from ρ_∞ are opposite, the action of the body forces is the same in both cases and they only differ with respect to the turbulent diffusion and the d.f.c. terms. Introducing the first-order approximation:

$$\overline{\rho u' v'} = \bar{\rho}\, \overline{u' v'} \left(1 + O \left(\frac{\rho''}{\bar{\rho}} \right)^2 \right)$$

(6.6) reduces to

$$\left(\bar{U} \frac{\partial \bar{U}}{\partial x} \right)_{\mathcal{L}} = \frac{(\bar{\rho} - \rho_\infty)_{\mathcal{L}}}{\bar{\rho}_{\mathcal{L}}} g_x - \underbrace{\left(\frac{1}{r} \frac{\partial r \overline{u' v'}}{\partial r} \right)_{r=0}}_{(a)} - \underbrace{\frac{\bar{U}_{\mathcal{L}}}{\bar{\rho}_{\mathcal{L}}} \left(\frac{\partial \overline{\rho u'}}{\partial x} \right)_{r=0}}_{(b)}, \tag{6.7}$$

from which three main qualitative results can be deduced.

(i) Focussing first on term (*a*), it is clear that the expression for the turbulent diffusion is exactly the same as for the constant-density case. In other words, (6.7) demonstrates that the density does not appear explicitly to modify the turbulent diffusion along the axis. Moreover, as already noted for the constant-density air jet, the value of the non-dimensional shear stress gradient along the axis is fairly close to 0.5 when $x \geqslant 50 R_0$. The same value was measured by Panchapakesan & Lumley (1993*b*) in a helium / air jet for $x \geqslant 100 R_0$. This result seems to suggest that this parameter should be insensitive to the density ratio in the far field. Thus the influence of the density ratio on the turbulent diffusion occurs near the exit. It does not appear explicitly in the mean momentum equation along the jet axis. Accordingly, this density effect results indirectly from the change of the shear stress gradient $\left[(1/r) \partial \left(r \overline{u' v'} \right) / \partial r \right]_{r=0}$ with density ratio. This suggests the introduction of a

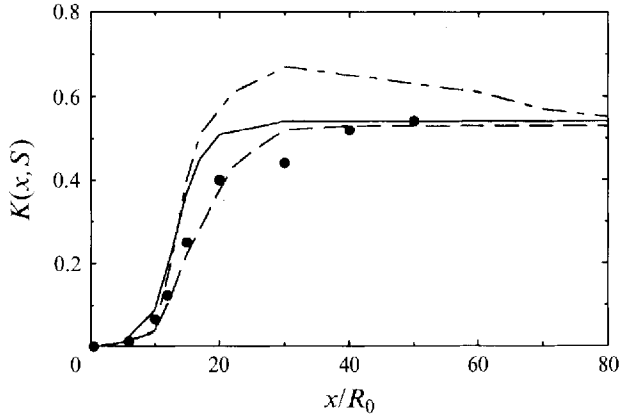

FIGURE 20. Density ratio effect on the non-dimensional shear stress gradient along the jet axis: – · –, $S = 0.57$; —, $S = 1$. – –, $S = 1.43$, model. •, $S = 1.43$, Exp. C79.

non-dimensional parameter:

$$K(x,S) = \lim_{r\to 0}\left[\frac{x}{r}\frac{\overline{u'v'}(r,S)}{\bar{U}_{\mathcal{L}}^2(x)}\right], \tag{6.8}$$

where $K(x,S)$ accounts for this kind of density effect on the turbulent diffusion. Using the previous predictions (§6.1) and Chassaing's experimental data (1979), the variation of $K(x,S)$ with x and S can be obtained and is given in figure 20. Compared with the constant-density jet, it is now clear, from figure 20, that the density ratio effect on the centreline mean velocity resulting from the turbulent diffusion, is to reduce the centreline decay rate when $S > 1$ and to increase it otherwise. From the results of the present study, this effect only occurs when $x < 80\,R_0$.

(ii) Let us turn now to the d.f.c. term (b) in (6.7). Since $\overline{\rho u'}$ is necessarily zero at the exit, it can be easily concluded from table 5 that, near the exit, $(\partial\overline{\rho u'}/\partial x)_{r=0}$ is positive when $S > 1$ and negative when $0 < S < 1$. Similarly, when x increases indefinitely, $\overline{\rho u'}$ tends to zero, so that further downstream, the signs are respectively opposite. Focussing on the region near the exit, the effect of the d.f.c. terms is to reduce the centreline decay rate of the velocity for a light jet ($0 < S < 1$) and to increase it for the heavy jet. The influence of S on both the (a) and (b) terms near the exit is sketched in figure 21. Introducing the asymptotic expressions for the d.f.c. terms, the previous effects can be refined, since for $S \to 0$ and $S \to +\infty$ the following are respectively obtained:

$$-\bar{U}_{\mathcal{L}}\left(\frac{\partial\overline{\rho u'}}{\partial x}\right)_{r=0} \approx \underbrace{+\left(\frac{\bar{U}}{\bar{C}}\frac{\overline{\rho u'}}{\bar{\rho}}\right)_{\mathcal{L}}\left[\frac{\partial\bar{C}}{\partial x}\right]_{r=0}}_{(b_l')} \underbrace{+\frac{\bar{U}_{\mathcal{L}}}{\bar{C}_{\mathcal{L}}\bar{\rho}_{\mathcal{L}}}\left[\frac{\partial\overline{\rho\gamma'u'}}{\partial x}\right]_{r=0}}_{(b_l'')},$$

$$-\bar{U}_{\mathcal{L}}\left(\frac{\partial\overline{\rho u'}}{\partial x}\right)_{r=0} \approx \underbrace{-\left(\frac{\bar{U}}{1-\bar{C}}\frac{\overline{\rho u'}}{\bar{\rho}}\right)_{\mathcal{L}}\left[\frac{\partial\bar{C}}{\partial x}\right]_{r=0}}_{(b_h')} \underbrace{-\frac{\bar{U}_{\mathcal{L}}}{(1-\bar{C}_{\mathcal{L}})\,\bar{\rho}_{\mathcal{L}}}\left[\frac{\partial\overline{\rho\gamma'u'}}{\partial x}\right]_{r=0}}_{(b_h'')}.$$

It can be verified that both (b_l') and (b_h') are always positive, and obviously $b_l'' > 0$

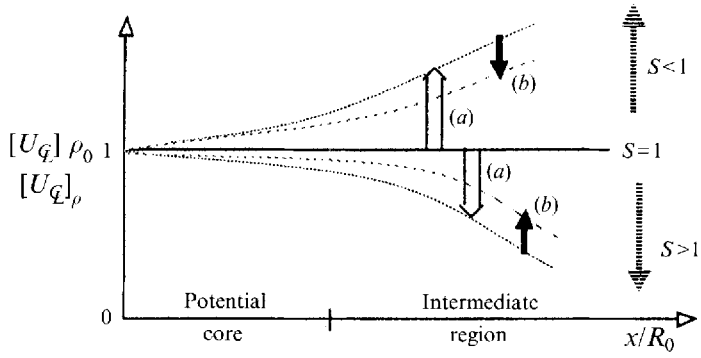

FIGURE 21. Density ratio effects on the mean velocity decay rate near the exit: (*a*) turbulent diffusion and (*b*) d.f.c. terms.

and $b_h'' < 0$ near the exit. Thus the main effect of the d.f.c. terms is due to the gradient of the mass-weighted mass-fraction velocity correlation along the jet axis.

(iii) Taking into account both the turbulent diffusion and the d.f.c. terms, it is clear that no symmetry about the constant-density case ($S = 1$) could exist between a heavy jet discharging downwards and a light one discharging upwards.

6.6. *Influence of the density ratio on the centreline mean mass-fraction decay rate*

The influence of the density ratio on the centreline decay rate of the mean mass-fraction can be examined in the same way. Discarding the d.f.c. contribution to the mean advection term along the axis, the mean mass-fraction transport equation (4.1*c*) simplifies along the jet axis to:

$$\left(\bar{\rho}\bar{U}\frac{\partial \bar{C}}{\partial x}\right)_{\mathcal{C}} = -\left[\frac{1}{r}\frac{\partial}{\partial r}\left(r\overline{\rho\gamma' v'}\right)\right]_{r=0} - \bar{U}_{\mathcal{C}}\left[\frac{\partial}{\partial x}\left(\overline{\rho\gamma'}\right)\right]_{r=0}.$$

Again, approximating $\overline{\rho\gamma' v'} \approx \bar{\rho}\,\overline{\gamma' v'}$, gives:

$$\left(\bar{U}\frac{\partial \bar{C}}{\partial x}\right)_{\mathcal{C}} = -\left[\frac{1}{r}\frac{\partial}{\partial r}\left(r\overline{\gamma' v'}\right)\right]_{r=0} - \frac{\bar{U}_{\mathcal{C}}}{\bar{\rho}_{\mathcal{C}}}\left[\frac{\partial}{\partial x}\left(\overline{\rho\gamma'}\right)\right]_{r=0}, \tag{6.9}$$

which is quite analogous to (6.7). However, till now there have been no measurements of the mass-fraction velocity correlation in variable-density turbulent round jets, so that the previous conclusions for the velocity centreline decay rate can only be considered as plausible conjectures for the mass-fraction one.

6.7. *Influence of the density ratio on the entrainment of the jet*

Let us consider again the mean momentum balance equation in the streamwise direction:

$$\bar{\rho}\left[\bar{U}\frac{\partial \bar{U}}{\partial x} + \left(\bar{V} + \frac{\overline{\rho v'}}{\bar{\rho}}\right)\frac{\partial \bar{U}}{\partial r}\right] = -\frac{1}{r}\frac{\partial}{\partial r}\left(r\overline{\rho u' v'}\right) + (\bar{\rho} - \rho_\infty)\,g - \bar{U}\frac{\partial \overline{\rho u'}}{\partial x} - \bar{V}\frac{\partial \overline{\rho u'}}{\partial r}.$$

Within the limit $r \to R$, where R denotes the outer edge of the jet ($\bar{U} \sim 0$, $\bar{\rho} \sim \rho_\infty$, $\bar{V} \sim V_E$, $\overline{\rho' u'} \sim \overline{\rho' v'} \sim 0$), this equation reduces to

$$V_E\left[\rho_\infty\frac{\partial \bar{U}}{\partial r} + \frac{\partial \overline{\rho u'}}{\partial r}\right]_{r=R} = -\left(\frac{1}{r}\frac{\partial r\,\overline{\rho u' v'}}{\partial r}\right)_{r=R}.$$

Since $\overline{\rho u'}$ is always zero outside the jet, it is concluded from table 5 that

$$0 < S < 1 : \quad \left[\frac{\partial \overline{\rho u'}}{\partial r}\right]_{r=R} > 0 \quad \text{and} \quad S > 1 : \quad \left[\frac{\partial \overline{\rho u'}}{\partial r}\right]_{r=R} < 0.$$

Consequently, the absolute value of the negative entrainment velocity V_E is greater when $0 < S < 1$ than it is when $S > 1$. Here again, introducing the asymptotic expressions for $\overline{\rho u'}$, a more explicit conclusion can be drawn, since

$$S \to 0 : \quad \left[\frac{\partial \overline{\rho u'}}{\partial r}\right]_{r=R} = \frac{-1}{\bar{C}} \left[\frac{\partial \overline{\rho\gamma' u'}}{\partial r}\right]_{r=R} + \frac{\overline{\rho\gamma' u'}}{\bar{C}^2} \left[\frac{\partial \bar{C}}{\partial r}\right]_{r=R},$$

$$S \to +\infty : \quad \left[\frac{\partial \overline{\rho u'}}{\partial r}\right]_{r=R} = \frac{1}{1-\bar{C}} \left[\frac{\partial \overline{\rho\gamma' u'}}{\partial r}\right]_{r=R} + \frac{\overline{\rho\gamma' u'}}{(1-\bar{C})^2} \left[\frac{\partial \bar{C}}{\partial r}\right]_{r=R},$$

from which it appears that the mean mass-fraction gradient contribution depends upon whether S is greater or lower than one.

6.8. *Influence of the density ratio on the restructuring of the flow*

An important feature of the flow is the restructuring from a fully developed pipe flow to a self-similar jet flow. In order to characterize the downstream extent of the restructuring region, we shall consider the turbulent kinetic energy balance along the jet axis. For a constant-density jet, it can be schematically written as follows:

$$\bar{U}_{\mathcal{L}} \left[\frac{\partial \bar{k}}{\partial x}\right]_{r=0} + Prod(x) - Diff(x) - Diss(x) \approx 0. \tag{6.10}$$

Near the exit, where the pipe jet is still wall dominated, the main production zone is located near the edge of the jet, at a radial distance of about R_0, and the production rate is not locally balanced in this region by the dissipation as shown by Sami (1967) for instance. Thus, a net amount of turbulent energy can be transferred towards the axis and consequently the centreline value increases. On the other hand in the self-preserving region, as shown by Wygnanski & Fiedler (1969) and Panchapakesan & Lumley (1993*a*), the absolute value of the maximum of the production rate is lower than that one of the dissipation and the centreline turbulent kinetic energy decreases. Consequently, a downstream location exists where the centreline turbulent kinetic energy is maximum. The abscissa of this section, denoted by X_{kmax}, will be used to characterize the downstream extent of the restructuring zone. According to (6.10), the value of X_{kmax} satisfies

$$Prod(X_{kmax}) \approx [Diff + Diss](X_{kmax}). \tag{6.11}$$

As measured by Chassaing (1979) in a turbulent pipe air jet, the value of X_{kmax} is about $18R_0$ for the present study. When the density varies, the variation of $\bar{k}_{\mathcal{L}}(x)$ is *qualitatively* unchanged, but as noted by Pitts (1991) the value of X_{kmax} appears to be a function of the density ratio. The experimental results of Sautet (1992) are plotted in figure 22 along with the values of the present study and the linear approximation $X_{kmax}/D_0 = 5.5S + 2.8$.

To provide a qualitative explanation for such a dependence, note that, for a variable-density jet, the approximate turbulent kinetic energy balance along the axis (6.10) is modified as follows:

$$\bar{U}_{\mathcal{L}} \left[\frac{\partial \bar{k}}{\partial x}\right]_{r=0} + Prod(x) - Diff(x) - Diss(x) \approx \left(\overline{\rho u'}\right)_{\mathcal{L}} g_x - \left(\overline{\rho u'}\,\bar{U}\right)_{\mathcal{L}} \left[\frac{\partial \bar{U}}{\partial x}\right]_{r=0}$$

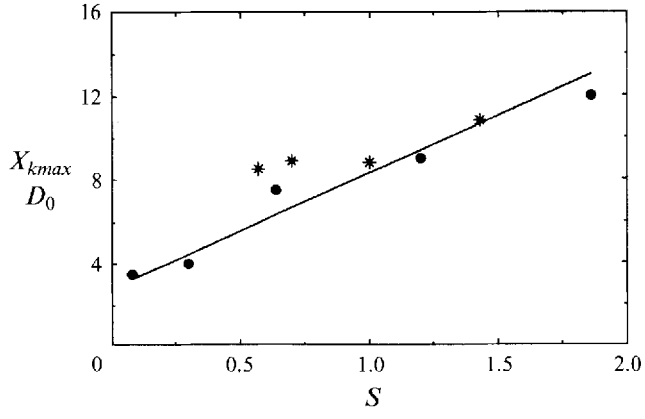

FIGURE 22. The restructuring lengthscale as a function of the density ratio: •, Sautet 1992; *, present study; —, $X_{kmax}/D_0 = 5.5S + 2.8$.

so that the characteristic restructuring length now satisfies the new condition

$$Prod\,(X_{kmax}) \approx [Diff + Diss]\,(X_{kmax}) + (\overline{\rho u'})_{\mathcal{C}_L} g_x - (\overline{\rho u'}\,\bar{U})_{\mathcal{C}_L} \left[\frac{\partial \bar{U}}{\partial x}\right]_{r=0}. \qquad (6.12)$$

Since the sign of the density–velocity correlation changes when the density ratio is greater or lower than unity, the gravity term is always a source term when the vertical directions of the heavy and light jets are inverted. On the other hand, the last term in (6.12) is positive when $S > 1$ and negative otherwise. Consequently, for the heavy jet both terms on the right-hand side in (6.12) act to reinforce the diffusion and the dissipation near the exit, hence increasing the value of X_{kmax}.

6.9. *Quantitative effects of the d.f.c. terms*

6.9.1. *Preliminaries*

The analytical discussion in §§ 6.2–6.8 provides some interesting results on the trends for how the d.f.c. terms modify the global features of the jet, and the differences between the heavy and light flow situations. However two shortcomings, at least, are still present: (i) the deductions are only qualitative, (ii) the deductions are likely to be inconclusive since the analysis is restricted to the d.f.c. terms independent of the second-order moments.

This point is crucial: when the density changes, such second-order correlations as $\overline{\rho f' g'}$ also introduce variable-density effects. Thus it must be questioned whether the previously analysed d.f.c. effects are not lower-order effects that could be masked by the variation of the second-order correlations with the density. This is the problem we address now.

From (6.1), three schematic situations can be introduced, which depend upon the amplitude of the variation range of the absolute value Γ of $\Gamma^S(C)$ with respect to S, whatever the values of C ($0 \leqslant C \leqslant 1$). Recalling that Γ is the ratio of the absolute value of the density–mass fraction correlation $\overline{\rho\gamma'}$ and the mass-weighted mass-fraction variance $\overline{\rho\gamma'^2}$, these situations correspond to:

(i) asymptotically low ratio : $\Gamma \in]0, \frac{1}{2}]$, for $2/3 \leqslant S \leqslant 3/2$;

(ii) bounded ratio : $\Gamma \in [\frac{1}{3}, 1]$, for $1/2 \leqslant S \leqslant 2/3$ or $3/2 \leqslant S \leqslant 2$;

(iii) asymptotically high ratio : $\Gamma \in [\frac{1}{2}, +\infty[$, for $S \leqslant 1/2$ or $S \geqslant 2$.

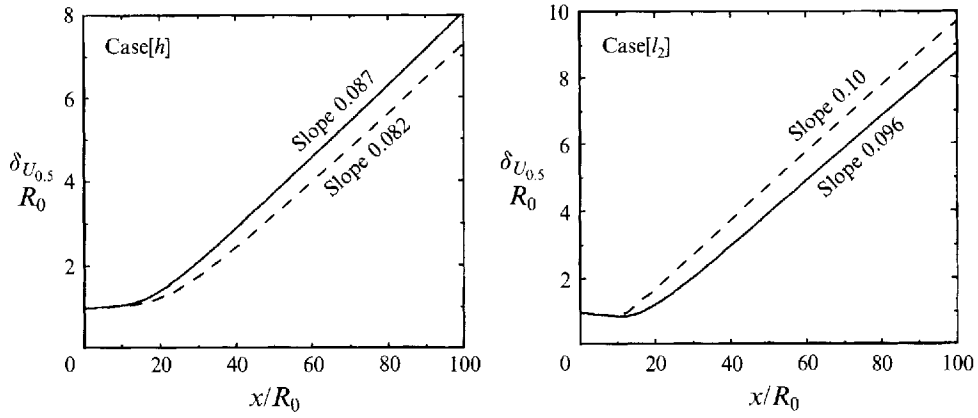

FIGURE 23. Influence of the d.f.c. terms on the spreading rate of the jet: —, with d.f.c. terms; – –, without d.f.c. terms.

For instance, the admissible variation range of Γ for a pure hydrogen jet discharging into air ($S = 0.07$) is [0.93, 13.3]. According to this classification, any quantitative conclusion about the comparative effects of the d.f.c. and second-order correlations is likely dependent on the situation under consideration. The present study is only concerned with the low-d.f.c. situation, and will be restricted to the [h] and [l_2] cases corresponding to $S = 1.43$ and $S = 0.57$ respectively. In order to obtain quantitative insight when scrutinizing the d.f.c. effects, and because no measurements are available, the numerical predictions are used. Actually, it is possible and very simple to solve the same set of modelled equations as previously, but where all the first-order d.f.c. terms are deliberately set equal to zero, i.e. $\overline{\rho u'} = \overline{\rho v'} = \overline{\rho w'} = \overline{\rho \gamma'} = 0$. Then, the comparison of the two predicted flows (with and without d.f.c. terms) directly brings out quantitative information on the influence of these terms.

6.9.2. *Jet spreading rate and mean decay rates*

Let us first examine the jet spreading rate based on the half-velocity width. As shown in figure 23, the slopes of the linear parts are only slightly changed by a factor of about 6% for the heavy jet and 4% for the light one (0.082 without d.f.c. terms, and 0.087 with d.f.c. terms for $S = 1.43$, 0.100 and 0.096, respectively, for $S = 0.57$).

Actually, as it can be observed in figure 23, most of the d.f.c. effects are located in the intermediate region of the jet. Consequently they mainly affect the virtual origins of the asymptotic linear far-field expressions. Thus, neglecting the d.f.c. terms leads to an overprediction of the location of the section where $\delta_{U_{0.5}} = 5R_0$ by a factor of 13% for the heavy jet, and an underprediction of the same parameter by 16% for the light jet. The influence of the density ratio on the mean velocity and mass-fraction centreline decay rates is quite similar to that just depicted, as shown in figures 24 and 25.

Here again, the following can be observed.

(i) No significant differences between the two predictions with and without d.f.c. terms exist near the exit ($x < 10R_0$). This is not surprising since, when the d.f.c. terms are present, they are prescribed equal to zero in the inlet section as a boundary condition (see § 5.1). Consequently, the downstream distance of about $10R_0$ corresponds to the vanishing of the inlet condition memory.

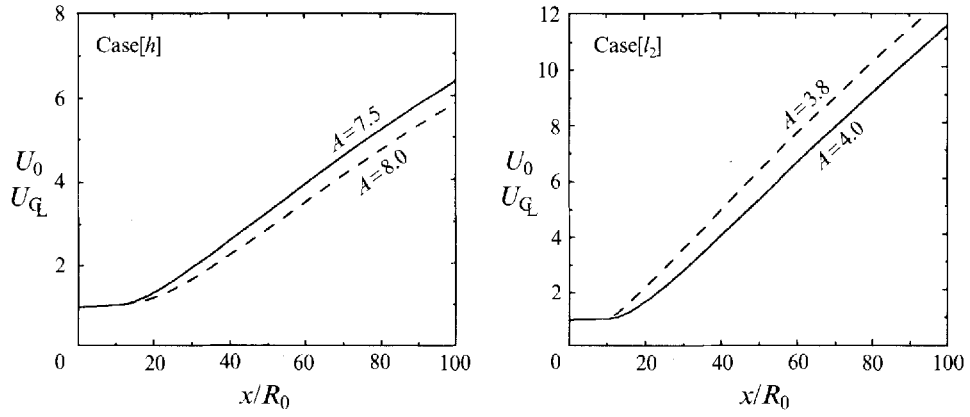

FIGURE 24. Influence of the d.f.c. terms on the mean centreline velocity. Same symbols as in figure 23.

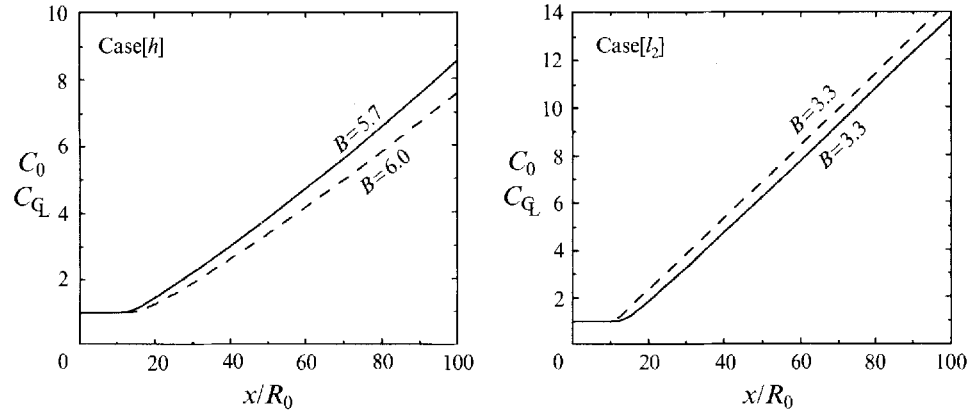

FIGURE 25. Influence of the d.f.c. terms on the mean centreline mass fraction. Same symbols as in figure 23.

(ii) The evolutions with and without d.f.c terms become different in the intermediate region $10 < x/R_0 < 30$, where the extremum of $\overline{\rho u'}$ is located. The situation is thus complex since the sign of the derivative $\left[\partial\overline{\rho u'}/\partial x\right]_{\mathcal{L}}$, which is the governing parameter of the effect of the d.f.c. terms (see § 6.6) is not constant in this region.

(iii) Further downstream ($x > 30R_0$), quasi-hyperbolic centreline decay rates are observed for both cases. When the d.f.c. terms are zero, the predicted flow is equivalent to that of a fictitious heavier jet when $S > 1$ and a fictitious lighter one when $0 < S < 1$.

(iv) Owing to the d.f.c. terms, the change in the values of the slopes of the linear parts of $1/\bar{U}_{\mathcal{L}}$ and $1/\bar{C}_{\mathcal{L}}$ is rather small.

(v) Most of the d.f.c. effect is concerned with the values of thevirtual origins x_U^* and x_C^*, in qualitative agreement with the measurements of Richards & Pitts (1993) on the influence of the density ratio S. The relative errors due to omitting the d.f.c. terms on the values of the parameters defined in expression (5.2) are reported in table 6.

Parameter	A	B	x_U^*	x_C^*
[h] $S = 1.43$	−9.5%	−5%	−70%	−70%
[l_2] $S = 0.57$	5%	≈ 0%	67%	51%

TABLE 6. Relative errors between the computed values with and without d.f.c. terms. The parameters refer to (5.2).

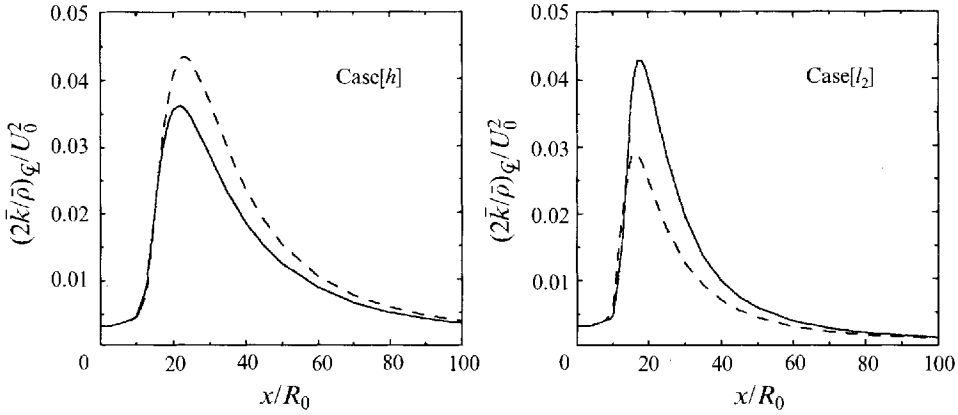

FIGURE 26. Influence of the d.f.c. terms on the turbulent kinetic energy along the axis. Same symbols as in figure 23.

To sum up, a triple conclusion can be drawn from this section:

(*a*) despite the rather small values of the d.f.c. terms ($|S - 1| \sim 0.4$, and $\Gamma = 0$ at $x = 0$) the predictions of the global behaviour of the jet are not insensitive to the presence of such density fluctuation correlations, but the amplitude of their effects is of course low;

(*b*) most of the d.f.c. effects occur within an intermediate region where the extremum of $\overline{\rho u'}$ along the axis is located;

(*c*) in the far field, the departure occurring in the intermediate region is not recovered. Thus, the rather natural conjecture of no influence of the d.f.c. terms in a region where the density difference between the jet and the surrounding air is vanishing is not quite correct.

6.9.3. *Turbulent kinetic energy and mass-fraction variance*

The turbulent kinetic energy and mass-fraction variance are given in figures 26 and 27 respectively for both [h] and [l_2] cases, with and without d.f.c. terms.

Concerning the variations of the turbulent kinetic energy along the axis of the heavy jet, two observations can be pointed out: (i) as anticipated in § 6.8, the location of the maximum is slightly shifted downstream when the d.f.c. terms are zero, (ii) in addition, the maximum value is overpredicted by about 20%, when the d.f.c. terms are zero. Turning now to the light jet, the conclusions are opposite, as shown by the analytical analysis.

The same type of conclusion also applies to the mass-fraction variance (figure 27). Finally, and as opposed to the mean quantities, it should be added that for such

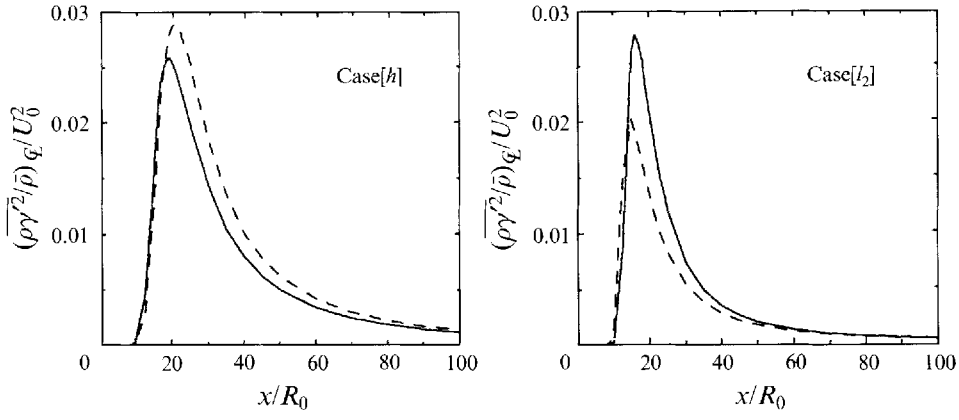

FIGURE 27. Influence of the d.f.c. terms on the mass-fraction variance along the axis. Same symbols as in figure 23.

second-order quantities, no significant influence of the d.f.c. terms is observed on the far-field values ($X = 100R_0$ for the present study).

7. Concluding remarks

The free turbulent mixing of two different-density gases in a jet flow is addressed with respect to (i) the formulation of the open set of equations, (ii) the analytical properties of the density fluctuation correlations, (iii) the qualitative influence of the d.f.c. terms on the global behaviour of the jet and (iv) the sensitivity of second-order modelling to such density correlations.

(*a*) The first conclusion concerns the new thermodynamical interpretation of the extra correlation terms which are introduced when averaging the divergence form of the variable-density Navier–Stokes equations. Making use of conventional fluctuations, it is shown that, due to the equation of state, the turbulent mass flux $\overline{\rho u_i'}$ and more generally, any density fluctuation correlation (d.f.c. term) $\overline{\rho f'}$ is exactly linked to the second-order correlation $\overline{\rho\gamma' u_i'}$ or $\overline{\rho\gamma' f'}$. These second-order correlations are mass-weighted moments of centred fluctuations. Exact transport equations of such second-order moments can be derived in which the d.f.c. terms appear separately. Thus the statistical averaging of the variable-density Navier–Stokes equations leads to a ternary analysis (mean, d.f.c and mass-weighted second- and higher-order correlations) of the single-point-moment open equations. Taking into account the explicit algebraic relationship between the d.f.c. terms and the mass-weighted second-order moment, no additional unknowns are introduced in the general formulation of the closure problem by the new approach.

(*b*) Secondly, some general analytical properties of the d.f.c. terms concerning the free turbulent mixing of two non-reactive gases have been identified. They can be summed up as follows:

(i) the first- to second-order mass-fraction and velocity fluxes ratios are equal, that is $\overline{\rho\gamma'}/\overline{\rho\gamma'^2} = \overline{\rho u_i'}/\overline{\rho\gamma' u_i'}$ and are both monotonically increasing functions with the mean mass fraction;

(ii) when the density ratio of the pure two-species S tends to zero (resp. $+\infty$) the previous function is equivalent to $-1/\bar{C}$ [resp. $1/(1-\bar{C})$];

(iii) the density–mass-fraction fluctuation correlation $\overline{\rho\gamma'}$ is always positive when $S > 1$, and negative when $0 < S < 1$;
(iv) the allowed variation range of the absolute value of the fluxes ratio $|\overline{\rho\gamma'}|/\overline{\rho\gamma'^2}$ only depends on the density ratio S.

(*c*) The third conclusion concerns the qualitative effects of the d.f.c. terms on the physical properties of the turbulent mixing in a free turbulent round jet. The main concluding points are:

(i) all the global properties of the jet (spreading rate, centreline decay rates, restructuring of turbulent kinetic energy) are sensitive to the d.f.c. terms ;

(ii) the turbulent mass fluxes $\overline{\rho u'}$ and $\overline{\rho v'}$ are positive when $S > 1$, and negative when $0 < S < 1$,

(iii) the d.f.c. effects are not symmetrical so that a heavy jet discharging downwards with $S = 1 + \alpha$, $\alpha > 0$ is not equivalent to a light one discharging upwards with $S = 1 - \alpha$.

(*d*) Finally the quantitative effects together with the sensitivity of second-order modelling to the d.f.c. terms have been demonstrated in a situation restricted to low inhomogeneous jet flows, where ratio of the inlet jet to ambient fluid density S is such that $|S - 1| \sim 0.4$. In this case, it is shown that:

(i) the first-order d.f.c. terms are significantly lower than the corresponding mean values product, $(\overline{\rho u'})_{max} \approx \bar{\rho}\bar{U}/200$ for instance;

(ii) the directions of variation in the jet cross-section of the mean products and the corresponding d.f.c. terms ($\bar{\rho}\bar{U}$ and $\overline{\rho u'}$ for instance) are quite different;

(iii) the d.f.c. effects occur within the first fifteen diameters from the exit and are not recovered further downstream;

(iv) even though the d.f.c. effects are obviously weak in the present situation, different predictions are observed depending upon whether these terms are disregarded or not ;

(v) finally, since $\overline{\rho f'}/\bar{\rho}$ and $\bar{F}$ do exhibit distinct evolutions, the results of the present study support the idea that, for the modelling procedure, the density fluctuation correlations should be treated separately and not included into a macroscopic mass-weighted mean value.

This work was supported by S.E.P. – C.N.E.S., under grant number 90.0018 C as part the "P.R.C. Moteurs Fusées" and the Region Midi-Pyrénées, under grant number 89 00946. The authors are very grateful to Professor H. Ha Minh for discussions on variable density jets and related topics. They would also like to thank the referees for their helpful comments on the manuscript.

Appendix A. Expressions for the S.L.J. approximations

From the mean equation of state (2.4*a*) one finds

$$\bar{\rho}\left(1 - a\bar{C}\right) = b + a\overline{\rho\gamma'}. \tag{A 1}$$

Hence

$$\bar{\rho} = \frac{b}{1 - a\bar{C}} + \frac{a}{1 - a\bar{C}}\overline{\rho\gamma'}.$$

Comparing with the S.L.J. development (3.5*a*):

$$\bar{\rho} = \frac{b}{1 - a\bar{C}} + O_1\left(\rho''\right)^2$$

results in

$$O_1\left(\rho''\right)^2 = \frac{a}{1-a\bar{C}}\overline{\rho\gamma'}. \tag{A 2}$$

Thus the second-order corrective term is proportional to the density/mass-fraction correlation and is always positive for the binary mixing situation. Subtracting the mean equation of state from the instantaneous one, it is found:

$$\rho'\left(1-a\bar{C}\right) = a\bar{\rho}\gamma' + a\rho'\gamma' - a\overline{\rho\gamma'}.$$

Now, from (A 1), it is clear that

$$\left(1-a\bar{C}\right) = \frac{b}{\bar{\rho}} + a\frac{\overline{\rho\gamma'}}{\bar{\rho}}.$$

Hence,

$$\rho'\left(\frac{b}{\bar{\rho}} + a\frac{\overline{\rho\gamma'}}{\bar{\rho}}\right) = a\bar{\rho}\gamma' + a\rho'\gamma' - a\overline{\rho\gamma'},$$

which is equivalent to

$$\frac{\rho'}{\bar{\rho}} = \frac{a}{b}\bar{\rho}\gamma' - \frac{a}{b}\overline{\rho\gamma'}\left(1+\frac{\rho'}{\bar{\rho}}\right) + \frac{a}{b}\rho'\gamma'. \tag{A 3}$$

Comparing with the corresponding S.L.J. development (3.5*b*):

$$\frac{\rho'}{\bar{\rho}} = \frac{a}{b}\bar{\rho}\gamma' + O_2\left(\frac{\rho''}{\bar{\rho}}\right)^2$$

results in

$$O_2\left(\frac{\rho''}{\bar{\rho}}\right)^2 = \frac{a}{b}\rho'\gamma' - \frac{a}{b}\overline{\rho\gamma'}\left(1+\frac{\rho'}{\bar{\rho}}\right). \tag{A 4}$$

The last result is directly obtained from (A 3) since multiplying by u_i' and averaging yields

$$\frac{\overline{\rho u_i'}}{\bar{\rho}} = \frac{a}{b}\bar{\rho}\overline{\gamma' u_i'} - \frac{a}{b}\overline{\rho\gamma'}\frac{\overline{\rho u_i'}}{\bar{\rho}} + \frac{a}{b}\overline{\rho'\gamma' u_i'}.$$

Hence

$$\overline{\rho u_i'} = \frac{a}{b}\bar{\rho}^2\overline{\gamma' u_i'} + O_3\left(\rho''\right)^3 \text{ with } O_3\left(\rho''\right)^3 = \frac{a}{b}\bar{\rho}\,\overline{\rho'\gamma' u_i'} - \frac{a}{b}\overline{\rho\gamma'}\,\overline{\rho u_i'}. \tag{A 5}$$

Similarly, it can be shown that:

$$\overline{\rho\gamma'} = \frac{a}{b}\bar{\rho}^2\overline{\gamma'^2} + O_4\left(\rho''\right)^3 \text{ with } O_4\left(\rho''\right)^3 = \frac{a}{b}\bar{\rho}\,\overline{\rho'\gamma'^2} - \frac{a}{b}\left(\overline{\rho\gamma'}\right)^2. \tag{A 6}$$

Appendix B. Relations between Favre's averages and centred fluctuation correlations

The instantaneous value of any function F may be written as follows:

$$F = \tilde{F} + f \quad \text{with} \quad \overline{f} \neq 0 \quad \text{and} \quad \overline{\rho f} = 0 \quad \text{(Favre)},$$
$$F = \bar{F} + f' \quad \text{with} \quad \overline{f'} = 0 \quad \text{and} \quad \overline{\rho f'} \neq 0 \quad \text{(Reynolds)}.$$

The mean values are obviously related by

$$\tilde{F} = \frac{\overline{\rho F}}{\bar{\rho}} = \bar{F} + \frac{\overline{\rho f'}}{\bar{\rho}}, \tag{B 1}$$

$$\bar{F} = \tilde{F} + \bar{f}. \tag{B 2}$$

It can be easily deduced that the relation between the fluctuations is

$$f' = f - \bar{f}, \tag{B 3}$$

from which it is obtained:

$$\overline{\rho f'} = -\bar{\rho}\bar{f}. \tag{B 4}$$

Applying (B 3) to the fluctuations of a new function G, multiplying by ρf and averaging, one obtains

$$\overline{\rho f g'} = \overline{\rho f g} - \bar{g}\overline{\rho f} \equiv \overline{\rho f g}. \tag{B 5}$$

Now, multiplying (B 3) by $\rho g'$ and averaging, it is deduced that

$$\overline{\rho f' g'} = \overline{\rho f g'} - \bar{f}\,\overline{\rho g'}. \tag{B 6}$$

Introducing (B 4) and (B 5), this leads to the relation between the second-order mass-weighted fluxes of the centred (Reynolds) fluctuations and the mass-weighted (Favre) fluctuations:

$$\overline{\rho f' g'} = \overline{\rho f g} + \frac{\overline{\rho f'}\,\overline{\rho g'}}{\bar{\rho}}. \tag{B 7}$$

Appendix C. Expression for the d.f.c. term according to a perfect gas law

Let us consider a variable-density fluid motion satisfying the perfect gas law:

$$P = r\rho T. \tag{C 1}$$

Introducing the Reynolds decomposition with $T = \bar{T} + \theta'$, one obtains

$$\bar{P} + p' = r\left(\bar{\rho}\bar{T} + \rho'\bar{T} + \rho\theta'\right). \tag{C 2}$$

Averaging (C 2), it is easily deduced that

$$\bar{P} = r\left(\bar{\rho}\bar{T} + \overline{\rho\theta'}\right)$$

and, by difference from (C 2),

$$p' = r\left(\rho'\bar{T} + \rho\theta' - \overline{\rho\theta'}\right).$$

Multiplying by any scalar centred fluctuation f' and averaging, it is obtained:

$$\overline{\rho f'}\left(\equiv \overline{\rho' f'}\right) = -\frac{1}{\bar{T}}\,\overline{\rho\theta' f'} + \frac{1}{r\bar{T}}\,\overline{p' f'}. \tag{C 3}$$

In this case, as compared with the free mixing situation, a pressure correlation term is introduced which should be taken into account in the modelling procedure like those occurring in the transport equations of second-order moments.

Appendix D. Expressions for second rank tensors and vectors of the modelled equations

The different expressions for the second-rank tensors and vectors introduced in the modelled form of the second-order-moment transport equations are

$$\bar{P}_{ij} = -\left(\overline{\rho u_i' u_l'}\,\frac{\partial \bar{U}_j}{\partial x_l} + \overline{\rho u_j' u_l'}\,\frac{\partial \bar{U}_i}{\partial x_l}\right),$$

$$\bar{Q}_{ij} = -\left(\overline{\rho u_i' u_l'}\,\frac{\partial \bar{U}_l}{\partial x_j} + \overline{\rho u_j' u_l'}\,\frac{\partial \bar{U}_l}{\partial x_i}\right),$$

$$\bar{Q} = \frac{1}{2}\bar{Q}_{ii} = \frac{1}{2}\bar{P}_{ii},$$

$$\bar{T}_{ij} = \frac{1}{2}\left(\frac{\partial \bar{U}_i}{\partial x_j} + \frac{\partial \bar{U}_j}{\partial x_i}\right), \qquad \bar{b}_{ij} = \frac{\overline{\rho u_i' u_j'}}{\bar{k}} - \frac{2}{3}\delta_{ij},$$

$$\bar{P}_{\gamma i} = -\left(\overline{\rho \gamma' u_l'}\,\frac{\partial \bar{U}_i}{\partial x_l} + \overline{\rho u_i' u_l'}\,\frac{\partial \bar{C}}{\partial x_l}\right).$$

REFERENCES

ABRAMOVICH, G. N., YAKOLEVSKY, D. V., SMIRNOVA, I. P., SECUNDOV, A. N. & KRASHENINNIKOV, S. YU. 1969 An investigation of turbulent jets of different gases in a general stream. *Aeronaut. Acta.* **18**, 229–240.

BAUER, P. T., ZUMWALT, G. W. & FILA, L. J. 1968 A numerical method and an extension of the Korst jet mixing theory for multispecie turbulent jet mixing. *AIAA Paper* 68 (112), 6th Aerospace Sciences Meeting, New York.

BEGUIER, C., DEKEYSER, I. & LAUNDER, B. E. 1978 Ratio of scalar and velocity dissipation time scales in shear flow turbulence. *Phys. Fluids* A **21**, 307–310.

BIRCH, A. D., BROWN, D. R., DODSON, M. G. & THOMAS, J. R. 1978 The turbulent concentration field of a methane jet. *J. Fluid Mech.* **88**, 431–449.

BOGULAWSKI, L. & POPIEL, C. O. 1979 Flow structure of the free round jet in the initial region. *J. Fluid Mech.* **90**, 531–539.

BRADBURY, L. J. S. 1965 The structure of a self-preserving turbulent plane jet. *J. Fluid Mech.* **23**, 31–64.

BRADBURY, L. J. S. 1967 Simple expressions for the spread of turbulent jets. *Aero. Q.* **18**, 133–142.

CHASSAING, P. 1977 Heat transfer from cylindrical anemometer probes in CO2–Air mixtures. *Phys. Fluids* **20**, 1260–1262.

CHASSAING, P. 1979 Mélange turbulent de gaz inertes dans un jet de tube libre. Thèse Doc. Sciences 42, Inst. Nat. Poly. de Toulouse.

CHASSAING, P. 1985 Une alternative à la formulation des équations du mouvement turbulent d'un fluide à masse volumique variable. *J. Méc. Théo. Appl.* **4**, 375–389.

CHASSAING, P. & HERARD, J. M. 1987 Second order modelling of a variable density turbulent mixing. *Sixth Symp. on Turbulent Shear Flows., Toulouse*, 17/8.

CHASSAING, P. & CHIBAT, M. 1988 Second order modelling of a variable density mixing layer. *Euromech. Coll. 237, Marseille, France.*

CHEN, C. J. & RODI, W. 1976 A review of experimental dada of vertical turbulent buoyant jets. *IIHM Rep.* 193.

CHEN, J. Y., GOULDIN, F. C. & LUMLEY, J. L. 1987 Second-order modelling of a turbulent nonpremixed H2-Air jet flame with intermittency and conditional averaging. *Combust. Sci. Tech.* **53**, 235–257.

CORRSIN, S. & UBEROI, M. S. 1949 Further experiments on flow and heat transfer in a heated turbulent air-jet. *NACA TN* 1865.

COUSTEIX, J. & AUPOIX, B. 1989 Three dimensional supersonic and hypersonic flows including separation. *AGARD-FDP-VKI Special Course*, pp. 1–53.

DONALDSON, C. DU P. & GRAY, K. E. 1966 Theoretical and experimental investigation of the compressible free mixing of two dissimilar gases. *AIAA J.* **4**, 2017–2025.

DOWLING, D. R. & DIMOTAKIS, P. E. 1990 Similarity of the concentration field of gas-phase turbulent jets. *J. Fluid Mech.* **218**, 109–141.

DRISCOLL, J. F., SCHEFER, R. W. & DIBBLE, R. W. 1982 Mass fluxes $\overline{\rho' u'}$ and $\overline{\rho' v'}$ measured in a turbulent nonpremixed flame. *Ninth Symp. on Combustion*, pp. 477–485. The Combustion Institute.

FAVRE, A. 1958 Equations statistiques des gaz turbulents. *C.R. Acad. Sci. Paris* **246**, 2573–3216.

FAVRE, A. 1965*a* Equations des gaz turbulents compressibles. I Formes générales. *J. Méc.* **4**, 361–390.

FAVRE, A. 1965*b* Equations des gaz turbulents compressibles. II Méthode des vitesses moyennes; Méthode des vitesses macroscopiques pondérées par la masse volumique. *J. Méc.* **4**, 390–421.

FAVRE, A. 1971 Equations statistiques aux fluctuations d'entropie, de concentration, de rotationnel dans les écoulements compressibles. *C.R. Acad. Sci. Paris* **273**, 1289–1294.

FAVRE, A. 1975 Equations statistiques des fluides turbulents compressibles. *Fifth Cong. Can. de Méc. Appl., New Brunswick Univ.*, pp. G3–G34.

FAVRE, A. 1992 Equations statistiques des fluides à masse volumique variable en écoulements turbulents. *Second Journées d'Etudes Ecoulements Turbulents Mane Volumique Variable*, Orléans, France.

FLORENT, P. 1966 Etude analytique et expérimentale des zones non établies des jets subsoniques turbulents à symétrie de révolution débouchant dans une atmosphère initialement immobile. Thèse Doct Etat. Univ. de Poitiers 60.

GEORGE, W. K. 1989 The self-preservation of turbulent flows and its relation to initial conditions and coherent structures. In *Advances in Turbulence* (ed W.K. George & R. Arndt), pp. 39–73. Hemisphere.

GRANDMAISON, E. W., RATHGEBER, D. E. & BECKER, H. A. 1982 Some characteristics of concentration fluctuation in free turbulent jets. *Can. J. Chem. Engng* **60**, 212–219.

HA MINH, H. & CHASSAING, P. 1978 Restructuration d'écoulements turbulents. *J. Méc.* **17**, 360–386.

HA MINH, H., LAUNDER, B. E. & MAC INNES, H. 1981 A new approach to the analysis of turbulent mixing in variable density flows. *3rd Symp. on Turbulent Shear Flows, Davis*, pp. 19619–19625.

HARRAN, G. 1994 Analyse physique, modélisation et simulation numérique des mécanismes de mélange dans les jets simples et coaxiaux turbulents. These 841, Inst. Nat. Poly. de Toulouse.

HERARD, J. M. 1986 Modélisation et calcul d'écoulements isothermes de gaz à densité variable. Thèse Doct.-Ing. 400, Inst. Nat. Poly. de Toulouse.

JONES, W. P. 1979 Models for turbulent flows with variable density and combustion. *Prediction Methods for Turbulent Flows.* VKI Lecture Series.

LARUE, J. C. & LIBBY, P. A. 1977 Measurements in the turbulent boundary layer with slot injection of helium. *Phys. Fluids* **20**, 192–202.

LARUE, J. C. & LIBBY, P. A. 1980 Further results related to the turbulent boundary layer with slot injection of helium. *Phys. Fluids* **23**, 1111–1118.

LAUNDER, B. E. & MORSE, A. 1977 Numerical prediction of axisymmetric free shear flows with a second-order Reynolds stress closure. *Symp. on Turbulent Shear Flows*, Pen State Univ. pp. 4/21–4/30.

O'CONNOR, COMFORT, E. H & CASS, L. A. 1966 Turbulent mixing of an axisymmetric jet of partially dissociated Nitrogen with ambient Air. *AIAA J.* **4**, 2026–2032.

PANCHAPAKESAN, N. R. & LUMLEY, J. L. 1993*a* Turbulence measurements in axisymmetric jets of air and helium. Part 1. Air jet. *J. Fluid Mech.* **246**, 197–223.

PANCHAPAKESAN, N. R. & LUMLEY, J. L. 1993*b* Turbulence measurements in axisymmetric jets of air and helium. Part 2. Helium jet. *J. Fluid Mech.* **246**, 225–247.

PATANKAR, S. V & SPALDING, D.B. 1970 *Heat and Mass Transfer in Boundary Layers*, 2nd edn. Intertext Books.

PITTS, W. M. 1986 Effects of global density and Reynolds number variations on mixing in turbulent, axisymmetric jets. *Int. Rep. AFOSR-ISSA-00012*, NTIS, Springfields, VA.

PITTS, W. M. 1991 Effects of global density ratio on the centreline mixing behavior of axisymmetric turbulent jets. *Exps. Fluids* **11**, 125–134.

REY, C. 1991 Ecoulements turbulents compressibles et variables aléatoires centrées. *Tenth Cong. Fran. Mec., Paris.*

REY, C. & ROSANT, J. M. 1990 Influence of density variations on small turbulent structures of temperature in strongly heated flows. *Ninth Intl Heat. Trans. Conf. Israel*, pp. 405–409.

RICHARDS, C. D. & PITTS, W. M. 1993 Global density effects on self-preservation behaviour of turbulent free jets. *J. Fluid Mech.* **254**, 417–435.

RODI, W. 1972 The prediction of free turbulent boundary layers by use of a two-equation model of turbulence. PhD thesis, Mech. Eng. Dept. Imperial College London.

SAMI, S. 1967 Turbulent energy in jet flow. *J. Fluid Mech.* **29**, 81–92.

SARH, B. 1990 Contribution à l'étude des jets turbulents à masse volumique variable et des flammes de diffusion turbulentes. Thèse Doct. d'Etat. Univ. Pierre et Marie Curie, Paris.

SAUTET, J. C. 1992 Effets des différences de densité sur le développement scalaire et dynamique des jets turbulents. Thèse, Univ. de Rouen.

SCHEFER, R. W. & DIBBLE, R. W. 1985 Rayleigh scattering measurements of mixture fraction in a turbulent nonreactive propane jet. *Sandia Rep.* SAND 85–8837.

SCHLÜNDER, E. U. 1971 Über die Ausbreitung turbulenter Freistrahlen. *Zeits. Flugwiss.* **19**, 108–113.

SFORZA, P. M. & MONS, R. F. 1978 Mass momentum and energy transport in turbulent free jets. *Intl J. Heat Mass Transfer* **21**, 371–384.

SHIH, T. H., LUMLEY J. L. & JANICKA, J. 1987 Second-order modelling of a variable-density mixing layer. *J. Fluid Mech.* **180**, 93–116.

SIESS, J. 1975 Etude, d'après la méthode de LUMLEY de la pénétration de la turbulence dans un milieu stratifié. Thèse Doc.-Ing., Univ. Aix-Marseille.

SO, R. M. C. & LIU T. M. 1986 On self-preserving, variable-density, turbulent free jets. *J. Appl. Maths Phys.* **37**, 538–558.

SO, R. M. C., ZHU, J. Y., OTÜGEN, M. V. & HWANG B. C. 1990 Some measurements in a binary gas jet. *Exps. Fluids* **9**, 237–284.

STEPOWSKI, D., LABBACI, K., CABOT, G. & TRINITE, M. 1988 Pseudo-self-similarity in the development of low density turbulent jet issuing in a coflow air. *Euromech 237, Marseille, France.*

THRING, M. W. & NEWBY, M. P. 1953 Combustion length of enclosed turbulent jet flames. *Flames and Fuel Jets*, 789–796.

VANDROMME, D. 1991 Turbulence modelling for compressible flows and implementation in Navier-Stokes solvers. 1991–02. VKI Lecture Series.

VANDROMME, D. & HA MINH, H. 1987 Coupling of turbulence models with Reynolds averaged compressible Navier-Stokes equations. Application to shock interactions. *IMA/SMAI Conf. Reading.*

WYGNANSKI, I. & FIEDLER, H. 1969 Some measurements in the self preserving jet. *J. Fluid Mech.* **38**, 577–612.

ZHU, J. Y., SO, R. M. C. & OTÜGEN, M. V. 1989 Mass transfer in a binary gas jet. *AIAA J.* **27**, 1132–1135.